Secondary Organic Aerosol (SOA) yields from NO₃ radical + isoprene based on nighttime aircraft power plant plume transects

Juliane L. Fry[1], Steven S. Brown[2,5], Ann M. Middlebrook[2], Peter M. Edwards[2,3,4], Pedro Campuzano-Jost[3,5], Douglas A. Day[3,5], José L. Jimenez[3,5], Hannah M. Allen[6], Thomas B. Ryerson[2], Ilana Pollack[2,3,a], Martin Graus[3,b], Carsten Warneke[2,3], Joost A. deGouw[3,5], Charles A. Brock[2], Jessica Gilman[2,3], Brian M. Lerner[2,3,c], William P. Dubé[2,3], Jin Liao[2,3,d], André Welti[2,3,e]

[1]Chemistry Department, Reed College, Portland, OR, USA
[2]Chemical Sciences Division, Earth System Research Laboratory, National Oceanic and Atmospheric Administration, Boulder, CO, USA
[3]Cooperative Institute for Research in Environmental Sciences, University of Colorado, Boulder, CO, USA
[4]Wolfson Atmospheric Chemistry Laboratories, Department of Chemistry, University of York, York, UK
[5]Department of Chemistry, University of Colorado, Boulder, CO, USA
[6]Division of Chemistry and Chemical Engineering, California Institute of Technology, Pasadena, CA, USA
[a]now at Department of Atmospheric Science, Colorado State University, Fort Collins, CO, USA
[b]now at Institute of Atmospheric and Cryospheric Sciences, University of Innsbruck, Austria.
[c]now at Aerodyne Research, Inc., Billerica, MA, USA
[d]now at Universities Space Research Association, Columbia, MD, USA and NASA Goddard Space Flight Center, Atmospheric Chemistry and Dynamic Laboratory, Greenbelt, MD, USA
[e]now at Leibniz Institute for Tropospheric Research, Department of Physics, Leipzig, Germany

Abstract

Nighttime reaction of nitrate radicals (NO₃) with biogenic volatile organic compounds (BVOC) has been proposed as a potentially important but also highly uncertain source of secondary organic aerosol (SOA). The southeast United States has both high BVOC and nitrogen oxide (NOₓ) emissions, resulting in a large model-predicted NO₃-BVOC source of SOA. Coal-fired power plants in this region constitute substantial NOₓ emissions point sources into a nighttime atmosphere characterized by high regionally widespread concentrations of isoprene. In this paper, we exploit nighttime aircraft observations of these power plant plumes, in which NO₃ radicals rapidly remove isoprene, to obtain field-based estimates of the secondary organic aerosol yield from NO₃ + isoprene. Observed in-plume increases in nitrate aerosol are consistent with organic nitrate aerosol production from NO₃ + isoprene, and these are used to determine molar SOA yields, for which the average over 9 plumes is 9%. Corresponding mass yields depend on the assumed molecular formula for isoprene-NO₃-SOA, but the average over 9 plumes is 27%, larger than those previously measured in chamber studies (12 – 14% after oxidation of both double bonds). Yields are larger for longer plume ages. This suggests that ambient aging processes lead more effectively to condensable material than typical chamber conditions allow. We discuss potential mechanistic explanations for this difference, including ambient peroxy radical lifetimes and heterogeneous reactions of NO₃-isoprene gas phase products. Future studies of aerosol composition from NO₃ radical + isoprene are needed to

43 better understand the oxidation chemistry producing this potentially important coupled
44 anthropogenic – biogenic source of SOA.

1 Introduction

46 Organic aerosol (OA) is increasingly recognized as a globally important component of the fine
47 particulate matter that exerts a large but uncertain negative radiative forcing on Earth's climate
48 (Myhre et al., 2013) and adversely affects human health around the world (Lelieveld et al.,
49 2015).This global importance is complicated by large regional differences in OA concentrations
50 relative to other sources of aerosol such as black carbon, sulfate, nitrate and sea salt. OA
51 comprises 20 – 50% of total fine aerosol mass at continental mid-latitudes, but more in urban
52 environments and biomass burning plumes, and up to 90% over tropical forests (Kanakidou et
53 al., 2005, Zhang et al., 2007). Outside of urban centers and fresh biomass burning plumes, the
54 majority of this OA is secondary organic aerosol (SOA) (Jimenez et al., 2009), produced by
55 oxidation of directly emitted volatile organic compounds followed by partitioning into the aerosol
56 phase. Forests are strong biogenic VOC emitters, in the form of isoprene (C_5H_8), monoterpenes
57 ($C_{10}H_{16}$), and sesquiterpenes ($C_{15}H_{24}$), all of which are readily oxidized by the three major
58 atmospheric oxidants, OH, NO_3, and O_3. The total global source of biogenic SOA from such
59 reactions remains highly uncertain, with a eview estimating it at 90 +/- 90 Tg C yr^{-1} (Hallquist et
60 al., 2009), a large fraction of which may be anthropogenically controlled (Goldstein et al., 2009,
61 Carlton et al., 2010, Hoyle et al., 2011, Spracklen et al., 2011). As most NO_3 arises from
62 anthropogenic emissions, OA production from NO_3 + isoprene is one mechanism that could
63 allow for the anthropogenic control of biogenic SOA mass loading.
64
65 Isoprene constitutes nearly half of all global VOC emissions to the atmosphere, with a flux of
66 ~600 Tg yr^{-1} (Guenther et al., 2006). As a result, accurate global biogenic SOA budgets depend
67 strongly on yields from isoprene oxidation. Recent global modeling efforts find that isoprene
68 SOA is produced at rates from 14 (Henze and Seinfeld 2006, Hoyle et al., 2007) to 19 TgC yr^{-1}
69 (Heald et al., 2008), which implies that it could constitute 27% (Hoyle et al., 2007) to 48%
70 (Henze and Seinfeld 2006) to 78% (Heald et al., 2008) of total SOA (based also on varying
71 estimates of total SOA burden in each study). More recent observational constraints on SOA
72 yield from isoprene find complex temperature-dependent mechanisms that could affect vertical
73 distributions (Worton et al., 2013) and suggest that isoprene SOA constitutes from 17% (Hu et
74 al., 2015) to 40% (Kim et al., 2015) up to 48% (Marais et al., 2016) of total OA in the
75 southeastern United States. This large significance comes despite isoprene's low SOA mass
76 yields – two recent observational studies estimated the total isoprene SOA mass yield to be
77 ~3% (Kim et al., 2015, Marais et al., 2016), and modeling studies typically estimate isoprene
78 SOA yields to be 4 to 10%, depending on the oxidant, in contrast to monoterpenes' yields of 10
79 to 20% and sesquiterpenes' yields of >40% (Pye et al., 2010). Furthermore, laboratory studies
80 of SOA mass yields may have a tendency to underestimate these yields, if they cannot access
81 the longer timescales of later-generation chemistry, or are otherwise run under conditions that
82 limit oxidative aging of first-generation products (Carlton et al., 2009).
83

84   Laboratory chamber studies of SOA mass yield at OA loadings of ~ 10 µg m^{-3} from isoprene
85   have typically found low yields from O_3 (1% (Kleindienst et al., 2007)) and OH (2% at low NO_x to
86   5% at high NO_x (Kroll et al., 2006, Dommen et al., 2009); 1.3% at low NO_x and neutral seed
87   aerosol pH but rising to 29% in the presence of acidic sulfate seed aerosol due to reactive
88   uptake of epoxydiols of isoprene (IEPOX) (Surratt et al., 2010)). One recent chamber study on
89   OH-initiated isoprene SOA formation focused on the fate of second-generation RO_2 radical
90   found significantly higher yields, up to 15% at low NO_x (Liu et al., 2016), suggesting that omitting
91   later-generation oxidation chemistry could be an important limitation of early chamber
92   determinations of isoprene SOA yields. Another found an increase in SOA formed with
93   increasing HO_2 to RO_2 ratios, suggesting that RO_2 fate could also play a role in the variability of
94   previously reported SOA yields.
95
96   For NO_3 oxidation of isoprene, early chamber experiments already pointed to higher yields (e.g.,
97   12% (Ng et al., 2008)) than for OH oxidation. Ng et al. (Ng et al., 2008) also observed chemical
98   regime differences: SOA yields were approximately two times larger when chamber conditions
99   were tuned such that first-generation peroxy radical fate was RO_2+RO_2 dominated than when it
100   was RO_2+NO_3 dominated. In addition, Rollins et al. (Rollins et al., 2009) observed a significantly
101   higher SOA yield (14%) from second-generation NO_3 oxidation than that when only one double
102   bond was oxidized (0.7%). This points to the possibility that later-generation, RO_2+RO_2
103   dominated isoprene + NO_3 chemistry may be an even more substantial source of SOA than
104   what current chamber studies have captured. Schwantes et al. (Schwantes et al., 2015)
105   investigated the gas-phase products of NO_3 + isoprene in the RO_2+HO_2 dominated regime and
106   found the major product to be isoprene nitrooxy hydroperoxide (INP, 75-78% molar yield), which
107   can photochemically convert to isoprene nitrooxy hydroxyepoxide (INHE), a molecule that might
108   contribute to SOA formation via heterogeneous uptake similar to IEPOX. Here again, multiple
109   generations of chemistry are required to produce products that may contribute to SOA.
110
111   Because the SOA yield appears to be highest for NO_3 radical oxidation, and isoprene is such an
112   abundantly emitted BVOC, oxidation of isoprene by NO_3 may be an important source of OA in
113   areas with regional NO_x pollution. Since the SOA yield with neutral aerosol seed appears to be
114   an order of magnitude larger than that from other oxidants, even if only 10% of isoprene is
115   oxidized by NO_3, it will produce comparable SOA to daytime photo-oxidation. For example,
116   Brown et al. (Brown et al., 2009) concluded that NO_3 contributed more SOA from isoprene than
117   OH over New England, where > 20% of isoprene emitted during the previous day was available
118   at sunset to undergo dark oxidation by either NO_3 or O_3. The corresponding contribution to total
119   SOA mass loading was 1 – 17% based on laboratory yields (Ng et al., 2017). Rollins et al.
120   (Rollins et al., 2012) concluded that multi-generational NO_3 oxidation of biogenic precursors was
121   responsible for one-third of nighttime organic aerosol increases during the CalNex-2010
122   experiment in Bakersfield, CA. In an aircraft study near Houston, TX, Brown et al. (Brown et al.,
123   2013) observed elevated organic aerosol in the nighttime boundary layer, and correlated vertical
124   profiles of organic and nitrate aerosol in regions with rapid surface level NO_3 radical production
125   and BVOC emissions. From these observations, the authors estimated an SOA source from
126   NO_3 + BVOCs within the nocturnal boundary layer of 0.05 – 1 µg m^{-3} h^{-1}. Carlton et al. (Carlton
127   et al., 2009) note the large scatter in chamber-measured SOA yields from isoprene

128 photooxidation and point throughout their review of SOA formation from isoprene to the likely
129 importance of poorly understood later generations of chemistry in explaining field observations.
130 We suggest that similar differences in multi-generational chemistry could explain the variation
131 among the (sparse) chamber and field observations of NO_3 + isoprene yields described in the
132 previous paragraph, and summarized in a recent review of NO_3 + BVOC oxidation mechanisms
133 and SOA formation (Ng et al., 2017).

134

135 The initial products of NO_3 + isoprene include organic nitrates, some of which will partially
136 partition to the aerosol phase. Organic nitrates in the particle phase ($pRONO_2$) are challenging
137 to quantify with online methods, due to both interferences and their often overall low
138 concentrations in ambient aerosol. Hence, field datasets to constrain modeled $pRONO_2$ are
139 sparse (Fisher et al., 2016, Ng et al., 2017). One of the most used methods in recent studies,
140 used also here, is quantification with the Aerodyne Aerosol Mass Spectrometer (AMS). Organic
141 nitrates thermally decompose in the AMS vaporizer and different approaches have been used to
142 apportion the organic fraction contributing to the total nitrate signal. Allan et al. (Allan et al.,
143 2004) first proposed the use of nitrate peaks at *m/z* 30 and 46 to distinguish various nitrate
144 species with the AMS. Marcolli et al. (Marcolli et al., 2006), in the first reported tentative
145 assignment of aerosol organic nitrate using AMS data, used cluster analysis to analyze data
146 from the 2002 New England Air Quality Study. In that study, cluster analysis identified two
147 categories with high *m/z* 30 contributions. One of these peaked in the morning when NO_x was
148 abundant and was more prevalent in plumes with lowest photochemical ages, potentially from
149 isoprene oxidation products. The second was observed throughout the diurnal cycle in both
150 fresh and aged plumes, and contained substantial *m/z* 44 contribution (highly oxidized OA). A
151 subsequent AMS laboratory and field study discussed and further developed methods for
152 separate quantification of organic nitrate (in contrast to inorganic nitrate) (Farmer et al., 2010). A
153 refined version of one of these separation methods, based on the differing NO_2^+/NO^+
154 fragmentation ratio for organic vs. inorganic nitrate, was later employed to quantify organic
155 nitrate aerosol at two forested rural field sites where strong biogenic VOC emissions and
156 relatively low NOx combined to make substantial organic nitrate aerosol concentrations ((Fry et
157 al., 2013, Ayres et al., 2015)). Most recently, Kiendler-Scharr et al. (Kiendler-Scharr et al., 2016)
158 used a variant of this method to conclude that across Europe, organic nitrates comprise ~40%
159 of submicron organic aerosol. Modeling analysis concluded that a substantial fraction of this
160 organic nitrate aerosol is produced via NO_3 radical initiated chemistry. Chamber studies have
161 employed this fragmentation ratio method to quantify organic nitrates (Fry et al., 2009, Rollins et
162 al., 2009, Bruns et al., 2010, Fry et al., 2011, Boyd et al., 2015), providing the beginnings of a
163 database of typical organonitrate fragmentation ratios from various BVOC precursors.

164

165 Measurements conducted at the SOAS ground site in Centreville, Alabama in 2013 found
166 evidence of significant organonitrate contribution to SOA mass loading. Xu et al. (Xu et al.,
167 2015) reported that organic nitrates constituted 5 to 12% of total organic aerosol mass from
168 AMS data applying a variant of the NO_2^+/NO^+ ratio method. Xu et al. (Xu et al., 2015) identify a
169 nighttime-peaking "LO-OOA" AMS factor which they attribute to mostly NO_3 oxidation of BVOC
170 (in addition to O_3 + BVOC). They estimated that the NO_3 radical oxidizes 17% of isoprene, 20%
171 of α-pinene, and 38% of β-pinene in the nocturnal boundary layer at this site. However, applying

172   laboratory-based SOA yields to model the predicted increase in OA, Xu et al. predict only 0.7 μg
173   m^{-3} of SOA would be produced, a factor of three lower than the measured nighttime LO-OOA
174   production of 1.7 μg m^{-3}. The more recent analysis of Zhang et al. (Zhang et al., 2018) found a
175   strong correlation of monoterpene SOA with the fraction of monoterpene oxidation attributed to
176   NO_3, even for non-nitrate containing aerosol, suggesting an influence of NO_3 even in pathways
177   that ultimately eliminate the nitrate functionality from the SOA, such as hydrolysis or NO_2
178   regeneration. Ayres et al. (Ayres et al., 2015) used a correlation of overnight organonitrate
179   aerosol buildup with calculated net NO_3 + monoterpene and isoprene reactions to estimate an
180   overall NO_3 + monoterpene SOA mass yield of 40 – 80%. The factor of two range in this
181   analysis was based on two different measurements of aerosol-phase organic nitrates. These
182   authors used similar correlations to identify specific CIMS-derived molecular formulae that are
183   likely to be NO_3 radical chemistry products of isoprene and monoterpenes, and found minimal
184   contribution of identified first-generation NO_3 + isoprene products to the aerosol phase (as
185   expected based on their volatility). Lee et al. (Lee et al., 2016) detected abundant highly
186   functionalized particle-phase organic nitrates at the same site, with apparent origin both from
187   isoprene and monoterpenes, and both daytime and nighttime oxidation, and estimated their
188   average contribution to submicron organic aerosol mass to be between 3 – 8 %. For the same
189   ground campaign, Romer et al. (Romer et al., 2016) found evidence of rapid conversion from
190   alkyl nitrates to HNO_3, with total alkyl nitrates having an average daytime lifetime of 1.7 hours.
191
192   Xie et al. (Xie et al., 2013) used a model constrained by observed alkyl nitrate correlations with
193   O_3 from the INTEX-NA/ICARTT 2004 field campaign to determine a range of isoprene nitrate
194   lifetimes between 4 and 6 hours, with 40-50% of isoprene nitrates formed by NO_3 + isoprene
195   reactions. Laboratory studies show that not all organic nitrates hydrolyze to HNO_3 equally
196   rapidly: primary and secondary organic nitrates were found to be less prone to aqueous
197   hydrolysis than tertiary organic nitrates (Darer et al., 2011, Hu et al., 2011, Boyd et al., 2015,
198   Fisher et al., 2016). This suggests that field-based estimates of the contribution of organic
199   nitrates to SOA formation could be a lower limit, if they are based on measurement of those
200   aerosol-phase nitrates. This is because if hydrolysis is rapid, releasing HNO_3 but leaving behind
201   the organic fraction in the aerosol phase, then that organic mass would not be accurately
202   accounted for as arising from nitrate chemistry. This was addressed in a recent modeling study
203   of SOAS (Pye et al., 2015) in which modeled hydrolysis products of particulate organic nitrates
204   of up to 0.8 μg m^{-3} additional aerosol mass loading in the southeast U.S. were included in the
205   estimate of change in OA due to changes in NO_x. Another recent GEOS-Chem modeling study
206   using of gas- and particle-phase organic nitrates observed during the $SEAC^4RS$ and SOAS
207   campaigns similarly finds $RONO_2$ to be a major sink of NO_x across the SEUS region (Fisher et
208   al., 2016, Lee et al., 2016).
209
210   Complementing these SOAS ground site measurements, the NOAA-led SENEX (Southeast
211   Nexus) aircraft campaign conducted 18 research flights focused in part on studying the
212   interactions between biogenic and anthropogenic emissions that form secondary pollutants
213   between 3 June and 10 July 2013 (Warneke et al., 2016). Flight instrumentation focused on
214   measurement of aerosol precursors and composition enable the present investigation of SOA
215   yields using this aircraft data set. Edwards et al. (Edwards et al., 2017) used data from the

216 SENEX night flights to evaluate the nighttime oxidation of BVOC, observing high nighttime
217 isoprene mixing ratios in the residual layer that can undergo rapid NO_3 oxidation when sufficient
218 NO_x is present. These authors suggest that past NO_x reductions may have been uncoupled
219 from OA trends due to NO_x not having been the limiting chemical species for OA production, but
220 that future reductions in NO_x may decrease OA if NO_3 oxidation of BVOC is a substantial
221 regional SOA source. Because isoprene is ubiquitous in the nighttime residual layer over the
222 southeastern United States and the NO_3 + isoprene reaction is rapid, NO_3 reaction will be
223 dominant relative to O_3 in places with anthropogenic inputs of NO_x (Edwards et al. (Edwards et
224 al., 2017) concludes that when NO_2/BVOC > 0.5, NO_3 oxidation will be dominant). Hence, a
225 modest NO_3 + isoprene SOA yield may constitute a regionally important OA source.
226
227 Several modeling studies have investigated the effects of changing NO_x on global and SEUS
228 SOA. Hoyle et al. (Hoyle et al., 2007) found an increase in global SOA production from 35 Tg yr^{-1}
229 ^{1} to 53 Tg yr^{-1} since preindustrial times, resulting in an increase in global annual mean SOA
230 mass loading of 51%, attributable in part to changing NO_x emissions. Zheng et al. (Zheng et al.,
231 2015) found only moderate SOA reductions from a 50% reduction in NO emissions: 0.9 – 5.6 %
232 for global NO_x or 6.4 – 12.0% for southeast US NO_x, which they attributed to buffering by
233 alternate chemical pathways and offsetting tendencies in the biogenic vs. anthropogenic SOA
234 components. In contrast, Pye et al. (Pye et al., 2015) find a 9% reduction in total organic aerosol
235 in Centreville, AL for only 25% reduction in NO_x emissions. A simple limiting-reagent analysis of
236 NO_3 + monoterpene SOA from power plant plumes across the United States found that between
237 2008 and 2011, based on EPA-reported NO_x emissions inventories, some American power
238 plants shifted to the NO_x-limited regime (from 3.5% to 11% of the power plants), and showed
239 that these newly NO_x-limited power plants were primarily in the southeastern United States (Fry
240 et al., 2015). The effect of changing NO_x on SOA burden is clearly still in need of further study.
241
242 Here, we present aircraft transects of spatially discrete NO_x plumes from electric generating
243 units (EGU), or power plants (PP), as a method to specifically isolate the influence of NO_3
244 oxidation. These plumes are concentrated and highly enriched in NO_x over a scale of only a
245 few km (Brown et al., 2012), and have nitrate radical production rates ($P(NO_3)$) 10 – 100 times
246 greater than those of background air. The rapid shift in $P(NO_3)$ allows direct comparison of air
247 masses with slow and rapid oxidation rates attributable to the nitrate radical, effectively isolating
248 the influence of this single chemical pathway in producing SOA and other oxidation products.
249 Changes in organic nitrate aerosol ($pRONO_2$) concentration and accompanying isoprene
250 titration enable a direct field determination of the SOA yield from NO_3 + isoprene.

251 **2 Field campaign and experimental and modeling methods**

252 The Southeast Nexus (SENEX: http://esrl.noaa.gov/csd/projects/senex/) campaign took place 3
253 June through 10 July 2013 as the NOAA WP-3D aircraft contribution to the larger Southeast
254 Atmospheric Study (SAS: http://www.eol.ucar.edu/field_projects/sas/), a large, coordinated
255 research effort focused on understanding natural and anthropogenic emissions, oxidation
256 chemistry and production of aerosol in the summertime atmosphere in the southeastern United
257 States. The NOAA WP-3D aircraft operated 18 research flights out of Smyrna, Tennessee,

258   carrying an instrument payload oriented towards elucidating emissions inventories and reactions
259   of atmospheric trace gases, and aerosol composition and optical properties (Warneke et al.,
260   2016). One of the major goals of the larger SAS study is to quantify the fraction of organic
261   aerosol that is anthropogenically controlled, with a particular focus on understanding how OA
262   may change in the future in response to changing anthropogenic emissions.
263
264   The subset of aircraft instrumentation employed for the present analysis of nighttime NO_3 +
265   isoprene initiated SOA production includes measurements used to determine NO_3 radical
266   production rate ($P(NO_3) = k_{NO2+O3}(T) [NO_2] [O_3]$), isoprene and monoterpene concentrations,
267   other trace gases for plume screening and identification, aerosol size distributions, and aerosol
268   composition. The details on the individual measurements and the overall aircraft deployment
269   goals and strategy are described in Warneke et al. (Warneke et al., 2016). Briefly, NO_2 was
270   measured by UV photolysis and gas-phase chemiluminescence (P-CL) and by cavity ringdown
271   spectroscopy, (CRDS), which agreed within 6%. O_3 was also measured by both gas-phase
272   chemiluminescence and CRDS and agreed within 8%, within the combined measurement
273   uncertainties of the instruments. Various volatile organic compounds were measured with
274   several techniques, including for the isoprene and monoterpenes of interest here, proton
275   reaction transfer mass spectrometry (PTR-MS) and canister whole air samples and post-flight
276   GC-MS analysis (iWAS/GCMS). A comparison of PTR-MS and iWAS/GCMS measurements of
277   isoprene during SENEX has high scatter due to imperfect time alignment and isoprene's high
278   variability in the boundary layer, but the slope of the intercomparison is 1.04 ((Warneke et al.,
279   2016); for more details on the VOC intercomparisons, see also Lerner et al., (Lerner et al.,
280   2017)). Acetonitrile from the PTRMS was used to screen for the influence of biomass burning.
281   Sulfur dioxide (SO_2) was used to identify emissions from coal-fired power plants. All gas-phase
282   instruments used dedicated inlets, described in detail in the supplemental information for
283   Warneke et al. (Warneke et al., 2016).
284
285   Aerosol particles were sampled downstream of a low turbulence inlet (Wilson et al., 2004), after
286   which they were dried by ram heating, size-selected by an impactor with 1 µm aerodynamic
287   diameter size cut-off, and measured by various aerosol instruments (Warneke et al., 2016). An
288   ultra-high-sensitivity aerosol sizing spectrometer (UHSAS, Particle Metrics, Inc., Boulder, CO
289   (Cai et al., 2008, Brock et al., 2011)) was used to measure the dry submicron aerosol size
290   distribution down to about 70 nm. Data for the UHSAS are reported at 1 Hz whereas AMS data
291   were recorded roughly every 10 seconds. The ambient (wet) surface areas were calculated
292   according to the procedures described in Brock et al., 2016 (Brock et al., 2016). A pressure-
293   controlled inlet (Bahreini et al., 2008) was employed to ensure that a constant mass flow rate
294   was sampled by a compact time-of-flight aerosol mass spectrometer (C-ToF-AMS) which
295   measured the non-refractory aerosol composition (Drewnick et al., 2005). The aerosol volume
296   transmitted into the AMS was calculated by applying the measured AMS lens transmission
297   curve (Bahreini et al., 2008) to the measured particle volume distributions from the UHSAS. For
298   the entire SENEX study, the mean, calculated fraction of aerosol volume behind the 1 micron
299   impactor that was transmitted through the lens into the AMS instrument was 97% (with ±4%
300   standard deviation), indicating that most of the submicron aerosol volume measured by the
301   sizing instruments was sampled by the AMS.

302
303 After applying calibrations and the composition-dependent collection efficiency following
304 Middlebrook et al. (Middlebrook et al., 2012), the limits of detection for the flight analyzed here
305 were 0.05 µg m^{-3} for nitrate, 0.26 µg m^{-3} for organic mass, 0.21 µg m^{-3} for ammonium, and 0.05
306 µg m^{-3} for sulfate, determined as three times the standard deviation of 10-second filtered air
307 measurements obtained for 10 minutes during preflight and 10 minutes during postflight (110
308 datapoints). Note that the relative ionization efficiency for ammonium was 3.91 and 3.87 for the
309 two bracketing calibrations and an average value of 3.9 was used for the flight analyzed here.
310 An orthogonal distance regression (ODR-2) of the volume from composition data (AMS mass
311 plus refractory black carbon) using a mass weighted density as described by Bahreini et al.
312 (Bahreini et al., 2009) versus the volume based on the sizing instruments (after correcting for
313 AMS lens transmission as above) had a slope of 1.06 for the entire SENEX study and 72% of
314 the data points were within the measurements' combined uncertainties of ±45% (Bahreini et al.,
315 2008). For the flight analyzed here, however, the same regression slope was 1.58, which is
316 slightly higher than the combined uncertainties. It is unclear why the two types of volume
317 measurements disagree more for this flight, since other flights during this field project compared
318 better; this does not change the conclusions of this work, but is discussed further in the
319 Supplemental Information and comparisons are shown for the plumes of interest in Fig. S1.
320
321 The C-ToF-AMS is a unit mass resolution (UMR) instrument and the mass spectral signals that
322 are characteristic of aerosol nitrate at m/z 30 and 46 (NO$^+$ and NO$_2^+$) often contain interferences
323 from organic species such as CH$_2$O$^+$ and CH$_2$O$_2^+$, respectively. Here, the m/z 30 and 46 signals
324 have been corrected for these interferences by using correlated organic signals at m/z 29, 42,
325 43, and 45 that were derived from high-resolution AMS measurements during the NASA
326 SEAC^{4}RS campaign that took place in the same regions of the SE US shortly after SENEX (see
327 Supplemental Information and Fig. S2). The corrections were applied to the individual flight
328 analyzed here from July 2. All of the corrections were well correlated with each other for the
329 SEAC^{4}RS dataset and we used the organic peak at m/z 29 (from CHO$^+$) and the peak at m/z 45
330 (from CHO$_2^+$), respectively, since those corrections were from peaks closest (in m/z) to those
331 being corrected. Once corrected, the nitrate mass concentrations in the final data archive for
332 this flight were reduced by 0-0.24 µg sm^{-3}, an average reduction of 0.11 µg sm^{-3} or 32% from
333 the initial nitrate mass concentrations. The organic interferences removed from the m/z 30 and
334 m/z 46 signals are linearly correlated with the total organic mass concentrations, corresponding
335 to an average 1.3% increase in the total organic mass.
336
337 The ratio of the corrected NO$_2^+$/NO$^+$ signals was then used to calculate the fraction of aerosol
338 nitrate that was organic (pRONO$_2$) or inorganic (ammonium nitrate) based on the method
339 described first in Fry et al. [27]. Here we used an organic NO$_2^+$/NO$^+$ ratio that was equal to the
340 ammonium nitrate NO$_2^+$/NO$^+$ ratio from our calibrations divided by 2.8. This factor was
341 determined from multiple datasets compiled by Day et al (Day et al., 2017), who discuss the
342 uncertainties of this approach in detail. The ammonium nitrate NO$_2^+$/NO$^+$ ratio was obtained
343 from the two calibrations on 30 June and 7 July that bracketed the flight on 2 July, which is
344 analyzed here. It was 0.514 and 0.488, respectively, and for all of the data from both
345 calibrations it averaged 0.490. Hence, the organic nitrate NO$_2^+$/NO$^+$ ratio was estimated to be

346   0.175. This is the first time, to our knowledge, that UMR measurements of aerosol nitrate have
347   been corrected with HR correlations and used to apportion the corrected nitrate into inorganic or
348   organic nitrate species.
349
350   The time since emission of intercepted power plant plumes was estimated from the slope of a
351   plot of O_3 against NO_2. For nighttime emitted NO_x plumes that consist primarily of NO (Peischl
352   et al., 2010), O_3 is negatively correlated with NO_2 due to the rapid reaction of NO with O_3 that
353   produces NO_2 in a 1:1 ratio:
354
355   $NO + O_3 \rightarrow NO_2 + O_2$ (R1)
356
357   Reaction R1 goes rapidly (NO pseudo first order loss rate coefficient of 0.03 s^{-1} at 60 ppb O_3) to
358   completion, so that all NO_x is present as NO_2, as long as the plume NO does not exceed
359   background O_3 after initial mixing of the plume into background air. Subsequent oxidation of
360   NO_2 via reaction (R2) leads to an increasingly negative slope of O_3 vs NO_2:
361
362   $NO_2 + O_3 \rightarrow NO_3 + O_2$ (R2)
363
364   Equation (1) then gives plume age subsequent to the completion of (R1) in terms of the
365   observed slope, m, of O_3 vs NO_2 (Brown et al., 2006).
366
367   $t_{plume} = \frac{ln[1 - S(m+1)]}{Sk_1\overline{O_3}}$ (1)
368
369   Here S is a stoichiometric factor that is chosen for this analysis to be 1 based on agreement of
370   plume age with elapsed time in a box model run initialized with SENEX flight conditions (see
371   below); k_2 is the temperature dependent bimolecular rate constant for $NO_2 + O_3$ (R2) and $\overline{O_3}$ is
372   the average O_3 within the plume.
373
374   We calculate plume ages using both a stoichiometric factor of 1 (loss of NO_3 and N_2O_5
375   dominated by NO_3 reactions) and 2 (loss dominated by N_2O_5 reactions)., although we note that
376   the chemical regime for $NO_3+N_2O_5$ loss may change over the lifetime of the plume, progressing
377   from 1 to 2 as the BVOC is consumed. We use $S=1$ values in the analysis that follows. Because
378   the more aged plumes are more likely to have S approach 2, this means that some of the older
379   plumes may have overestimated ages. Fig. S3 in the Supplemental Information shows the
380   plume age calculated by Eq. 1 using modeled NO_x, NO_y and O_3 concentrations for $S=1$ and
381   $S=2$, from nighttime simulations of plume evolution using an observationally constrained box
382   model. This confirms that for nighttime plumes, $S=1$ plume ages match modeled elapsed time
383   well. The model used for this calculation, and those used to assess peroxy radical lifetimes and
384   fates in Section 4.3, was the Dynamically Simple Model of Atmospheric Chemical Complexity
385   (DSMACC (Emmerson and Evans 2009)) containing the Master Chemical Mechanism v3.3.1
386   chemistry scheme (Jenkin et al., 2015). More details on the model approach are provided in the
387   SI.

3 Nighttime flight selection

There were three nighttime flights (takeoffs on the evenings of 19 June, 2 July, and 3 July, 2013, local time) conducted during SENEX, of which one (2 July) surveyed regions surrounding Birmingham, Alabama, including multiple urban and power plant plume transects. As described in the introduction, these plume transects are the focus of the current analysis since they correspond to injections of concentrated NO (and subsequently high $P(NO_3)$) into the regionally widespread residual layer isoprene. The nighttime flight on 3 July, over Missouri, Tennessee and Arkansas sampled air more heavily influenced by biomass burning than biogenic emissions. The 19 June night flight sampled earlier in the evening, in the few hours immediately after sunset, and sampled more diffuse urban plume transects that had less contrast with background air. Therefore, this paper uses data exclusively from the 2 July flight, in which 9 transects of well-defined NO_x plumes from power plants emitted during darkness can be analyzed to obtain independent yields measurements.

A map of the 2 July flight track is shown in Fig. 1a. After takeoff at 8:08 pm local Central Daylight Time on 2 July, 2013 (1:08 am UTC 3 July, 2016), the flight proceeded towards the southwest until due west of Montgomery, AL, after which it conducted a series of east-west running tracks while working successively north toward Birmingham, AL. Toward the east of Birmingham, the aircraft executed overlapping north-south tracks at six elevations to sample the E. C. Gaston power plant. During the course of the flight, concentrated NO_x plumes from the Gaston, Gorgas, Miller and Greene City power plants were sampled. Around 1:30 and 2:30 AM Central Daylight Time (5:30 and 6:30 am UTC), two transects of the Birmingham, AL urban plume were measured prior to returning to the Smyrna, TN airport base.

The flight track is shown colored by the nitrate radical production rate, $P(NO_3)$, to show the points of urban and/or power plant plume influence:

$$P(NO_3) = k_2(T)\,[NO_2][O_3] \tag{2}$$

Here, k_2 is again the temperature-dependent rate coefficient for reaction of $NO_2 + O_3$ (Atkinson et al., 2004), and the square brackets indicate number densities. Fig. 1b further illustrates the selection of power plants plumes: sharp peaks in $P(NO_3)$ are indicative of power plant plume transects, during which isoprene mixing ratios also are observed to drop from the typical regional residual layer background values of ~ 1 ppb, indicative of loss by NO_3 oxidation (an individual transect is shown in more detail below in Fig. 2). Also shown in Fig. 1b are measured concentrations of isoprene and monoterpenes throughout the flight, showing substantial residual layer isoprene and supporting the assumption that effectively all NO_3 reactivity is via isoprene (see calculation in next section). Residual layer concentrations of other VOCs that could produce SOA (e.g., aromatics) are always below 100 pptv, and their reaction rates with NO_3 are slow. Edwards *et al*. (Edwards et al., 2017) have shown that NO_3 and isoprene mixing ratios for this and other SENEX night flights exhibit a strong and characteristic anticorrelation that is consistent with nighttime residual layer oxidation chemistry.

431 **1a**

432 **1b**
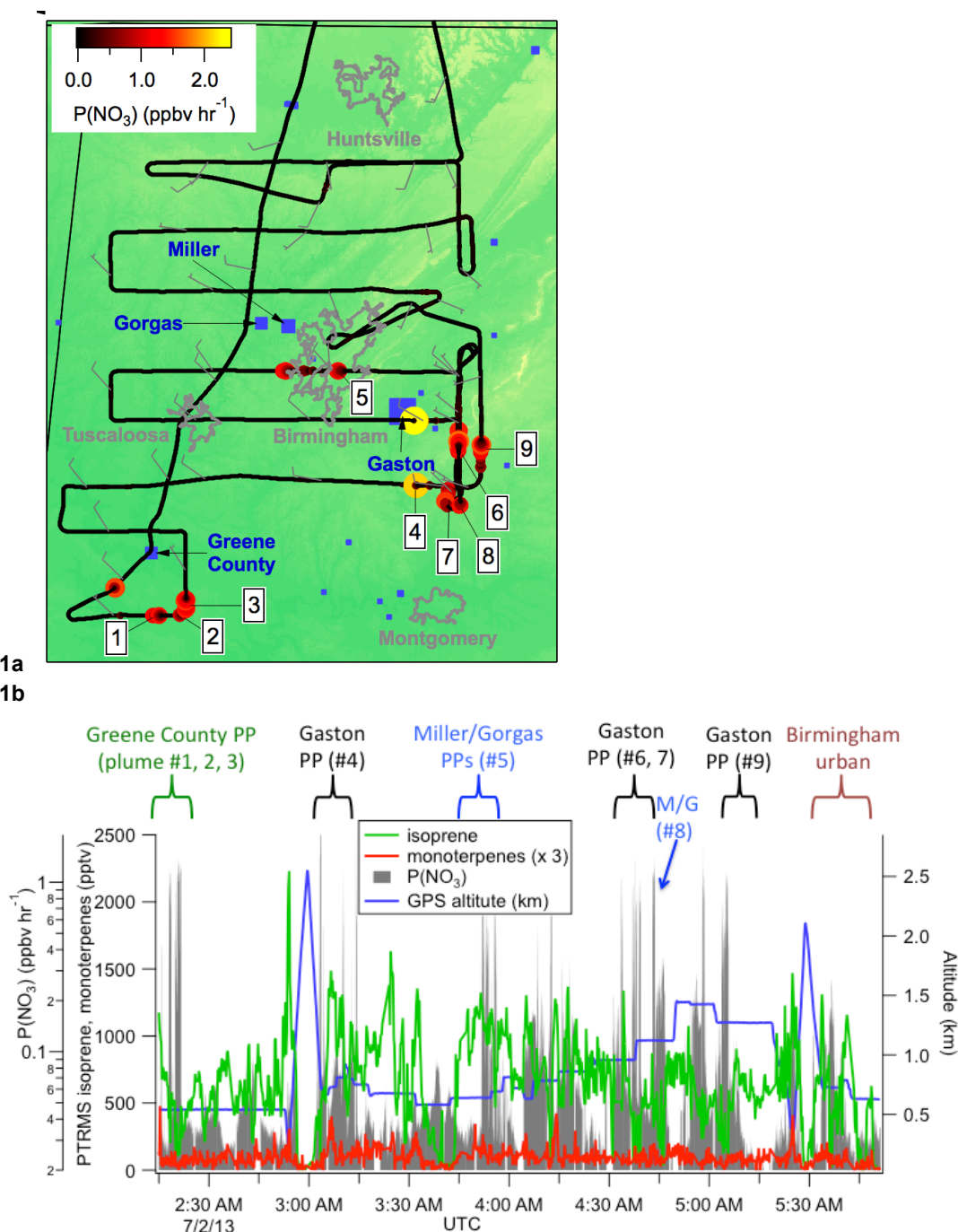
433

434 **Figure 1a.** Map of northern Alabama, showing the location of the flight track of the 2 July 2013

435 night flight used in the present analysis, with plume numbers labeled and wind direction shown.

436 Although the wind direction changed throughout the night, these measurements enable us to

437   attribute each plume to a power plant source (see labels in Figure 1b and Table 2). Color scale
438   shows $P(NO_3)$ based on aircraft-measured $[NO_2]$ and $[O_3]$, while power plants discussed in the
439   text are indicated in blue squares with marker size scaled to annual NO_x emissions for 2013
440   (scale not shown). Isoprene emissions are widespread in the region (Edwards et al., 2017).
441   **Figure 1b** shows time series data from the same flight, with plume origins and numbers labeled,
442   showing aircraft-measured isoprene and monoterpene concentrations, altitude, and $P(NO_3)$
443   determined according to Eq. 2 (log scale), showing that the isoprene was uniformly distributed
444   (mixing ratios often in excess of 1 ppbv), while the more reactive monoterpenes were present at
445   mixing ratios below 100 ppt except at the lowest few hundred meters above ground in the
446   vertical profiles (not used in the present analysis). Figure 1b also shows that sharp peaks in
447   nitrate radical production rate occur both at the lowest points of these vertical profiles, when the
448   aircraft approached the surface, but also frequently during periods of level flight in the residual
449   layer, which correspond to the power plant plume transects analyzed in this paper.

450   # 4 Results

451   ## 4.1 Selection of plumes
452   Figure 2 shows a subset of the July 2 flight time series data, illustrating three NO_x plumes used
453   for analysis. The large NO_3 source and isoprene loss was accompanied by an increase in
454   organic nitrate aerosol mass, which we attribute to the NO_3 + isoprene reaction based on prior
455   arguments. We observed each plume as a rapid and brief perturbation to background
456   conditions, of order 10 – 50 sec., or 1 – 5 km in spatial scale. Each plume's perturbed
457   conditions can correspond to different plume ages, depending on how far downwind of the
458   power plant the plume transect occurred.

459
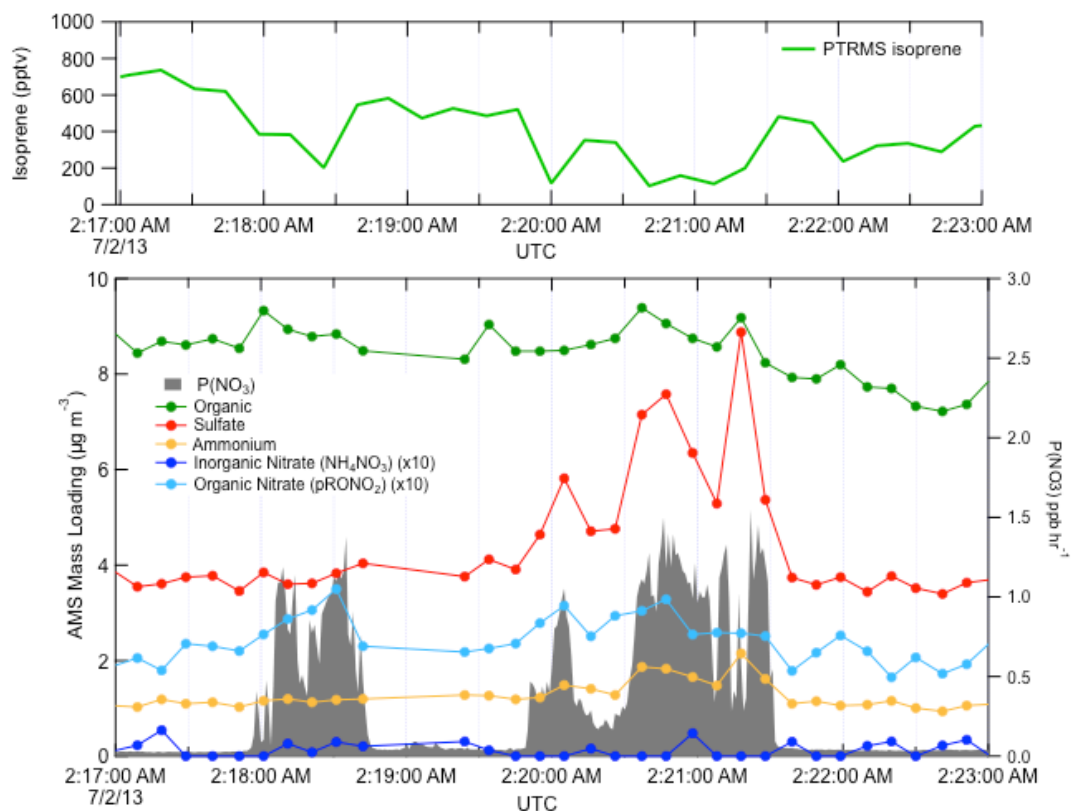
460

461 **Figure 2.** Three representative plume transect observations from the 2 July 2013 flight (plumes
462 are identified by the peaks in $P(NO_3)$, listed in Table 1 at times 02:18, 02:20, and 02:21 UTC).
463 Note the difference in sulfate enhancement in the three plumes, which is largest in the third
464 plume, and is accompanied by increases in ammonium. In all three cases, the isoprene
465 concentration drops in the plumes, accompanied by a clear increase in organic nitrate, no
466 changes in the inorganic nitrate, and a modest changes in organic aerosol mass concentrations.

467

468 Candidate plumes were initially identified by scanning the time series flight data for any period
469 where the production rate of nitrate radical ($P(NO_3)$) rose above 0.5 ppbv hr^{-1}. For each such
470 period, a first screening removed any of these candidate plumes that occurred during missed
471 approaches or other periods where radar altitude above ground level (AGL) was changing,
472 because in the stratified nighttime boundary layer structure, variations in altitude may result in
473 sampling different air-masses, rendering the adjacent out of plume background not necessarily
474 comparable to in-plume conditions. A second criterion for rejection of a plume was missing
475 isoprene or AMS data during brief plume intercepts. No selected plumes on July 2 showed
476 enhanced acetonitrile or refractory black carbon, indicating no significant biomass burning
477 influence. Finally, two plumes downwind of the Gaston power plant (at 03:10 and 03:14) were
478 removed from the present analysis, because (03:10) the background isoprene was changing

479   rapidly, preventing a good baseline measurement, and (03:14) there was no observed decrease
480   in isoprene concentration in-plume (as well as no increase in nitrate aerosol). The 03:14 plume
481   was apparently too recently emitted to have undergone significant nighttime reaction; its O_3/NO_2
482   slope was unity to within the combined measurement error of O_3 and NO_2 (Eq. 1). After this
483   filtering, there are 9 individual plume observations for determination of NO_3 + isoprene SOA
484   yields (see Table 1). The rapid increases in $P(NO_3)$ appeared simultaneously with significant
485   decreases in isoprene and increases in aerosol nitrate. The aerosol and isoprene
486   measurements (taken at data acquisition rates < 1 Hz) were not exactly coincident in time which
487   leads to some uncertainty in the yield analysis below.
488
489   Derivation of SOA yields from observed changes in isoprene and aerosol mass in plumes
490   depends on two conditions, and has several caveats that will be discussed in the text that
491   follows (see Table 3 below for a summary of these caveats). The two conditions are: (1) that the
492   majority of VOC mass consumed by NO_3 in plumes is isoprene (rather than monoterpenes or
493   other VOC), and then either or both (2a) that the change in aerosol organic mass concentration
494   during these plumes is due to NO_3 + isoprene reactions, and/or (2b) that the change in aerosol
495   nitrate mass concentration is due to NO_3 + isoprene reactions. There are separate
496   considerations for each of these conditions.
497
498   For the first condition, we note that the isoprene to monoterpenes ratio just outside each plume
499   transect was always high (a factor of 10 to 70, on average 26). With the 298 K NO_3 rate
500   constants of ~ 5 × 10^{-12} cm^3 $molec^{-1}$ s^{-1} for monoterpenes and 6.5 × 10^{-13} cm^3 $molec^{-1}$ s^{-1} for
501   isoprene (Calvert et al., 2000), isoprene (~ 2 ppb) will always react faster with nitrate than
502   monoterpenes (~ 0.04 ppbv). At these relative concentrations, even if all of the monoterpene is
503   oxidized, the mass of hydrocarbon conversion will be much larger for isoprene. Contribution to
504   aerosol by N_2O_5 uptake is also not important in these plumes. Edwards et al. (Edwards et al.,
505   2017) calculated the sum of NO_3 and N_2O_5 loss throughout this flight and showed that it is
506   consistently NO_3+BVOC dominated (Fig. S4 of that paper). As isoprene depletes, N_2O_5 uptake
507   will increasingly contribute to NO_3 loss, but as shown below, we are able to rule out a
508   substantial source of inorganic nitrate for most plumes. We also know that despite increased
509   OH production in-plume, the isoprene loss is still overwhelming dominated by NO_3 (Fig. S5 in
510   Edwards, et al. (Edwards et al., 2017)) .
511
512   The second condition requires that we can find an aerosol signal that is attributable exclusively
513   to NO_3 + isoprene reaction products, whether it be organic aerosol (OA) or organic nitrate
514   aerosol ($pRONO_2$) mass loading, or both. We note that the ratio of in-plume aerosol organic
515   mass increase to $pRONO_2$ mass increase is noisy (see discussion below at Fig. 6), but indicates
516   an average in-plume ΔOA to $\Delta pRONO_2$ ratio of about 5. The large variability is primarily due to
517   the fact that the variability in organic aerosol mass between successive 10-second data points
518   for the entire flight is quite large (of order 0.75 $\mu g\ m^{-3}$) and comparable to many of the individual
519   plume ΔOA increases, far exceeding the expected organonitrate driven increases in OA, which
520   are roughly twice the $pRONO_2$ mass increases. It is also possible that in these plumes, where
521   total aerosol mass is elevated, semivolatile organic compounds may re-partition to the aerosol
522   phase, contributing a non-$pRONO_2$ driven variability in ΔOA. For example, if some gas phase

523 IEPOX is present in the residual layer, it may be taken up into the highly acidic aerosol from the
524 power plants. Alternatively, very polar gas-phase compounds could partition further into the
525 higher liquid water associated with the sulfate in the plume. Therefore, in-plume organic aerosol
526 increases cannot be attributed clearly to NO_3 + isoprene SOA production, so we do not use
527 them in the SOA yield calculations.

528

529 This leaves consideration 2b, whether all increase in nitrate mass is due to NO_3 + isoprene
530 reactions. Here we must evaluate the possibility of inorganic nitrate aerosol production in these
531 high-NO_x plumes. Fine-mode aerosol inorganic nitrate can be formed by the (reversible)
532 dissolution of $HNO_{3(g)}$ into aqueous aerosol. In dry aerosol samples, inorganic nitrate is typically
533 in the form of ammonium nitrate (NH_4NO_3), when excess ammonium is available after
534 neutralization of sulfate as $(NH_4)_2SO_4$ and $NH_4(HSO_4)$. Because of the greater stability of
535 ammonium sulfate salt relative to ammonium nitrate, in high-sulfate plumes with limited
536 ammonium, inorganic nitrate aerosol will typically evaporate as $HNO_{3(g)}$ (Guo et al., 2015)
537 (reaction R3):

538

539 $2NH_4NO_{3(aq)} + H_2SO_{4(aq)} \rightleftarrows (NH_4)_2SO_{4(aq)} + 2HNO_{3(g)}$ (R3)
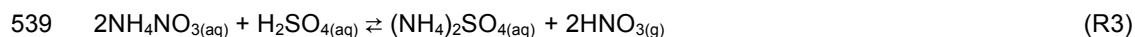
540

541 Inorganic nitrate can also form when crustal dust (e.g. $CaCO_3$) or seasalt (NaCl) are available.
542 Uptake of HNO_3 is rendered favorable by the higher stability of nitrate mineral salts, evaporating
543 CO_2 or HCl.

544

545 There are several lines of evidence that the observed nitrate aerosol is organic and not
546 inorganic. First, examination of the NO_2^+/NO^+ (interference-corrected m/z 46:m/z 30) ratio
547 measured by the aircraft AMS (Fig. 3) shows a ratio throughout the July 2 flight, including the
548 selected plumes, that is substantially lower than that from the bracketing ammonium nitrate
549 calibrations. This lower AMS measured NO_2^+/NO^+ ratio has been observed for organic nitrates
550 (Farmer et al., 2010), and some mineral nitrates (e.g. $Ca(NO_3)_2$ and $NaNO_3$, (Hayes et al.,
551 2013)), which are not important in this case because aerosol was dominantly submicron. As
552 described above, we can separate the observed AMS nitrate signal into $pRONO_2$ and inorganic
553 nitrate contributions. These mass loadings are also shown in Fig. 3, indicating dominance of
554 $pRONO_2$ throughout the flight.

555
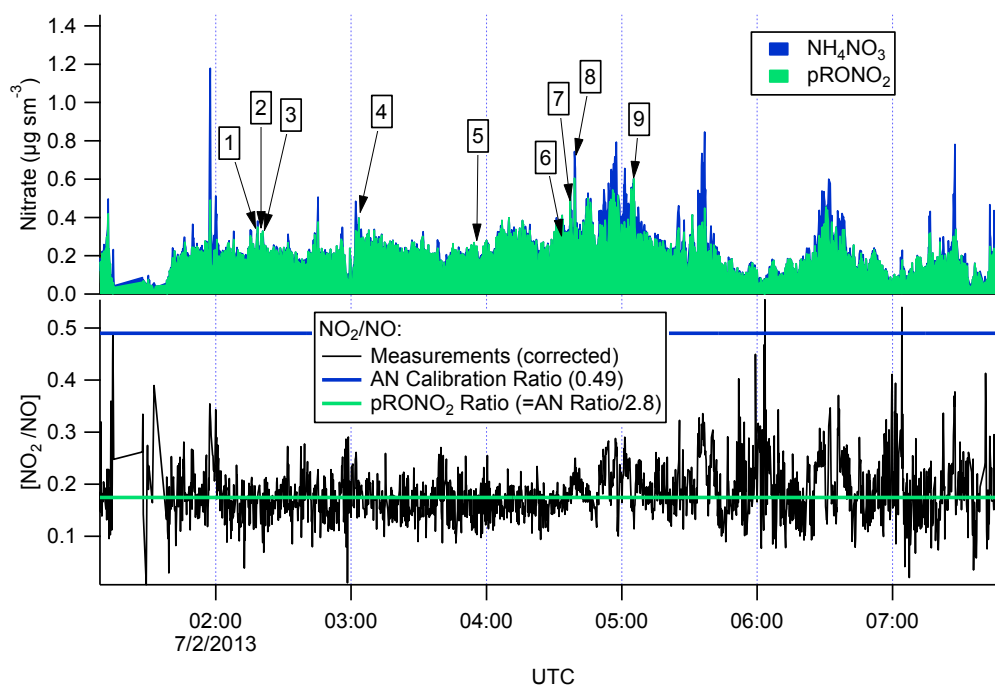
556
557 **Figure 3.** For the flight under consideration, the estimated relative contributions of ammonium
558 and organic nitrate to the total corrected nitrate signal (top panel) was calculated from the ratios
559 of the corrected peaks at *m/z* 30 and 46 (lower panel). Each of the plumes is identified here by
560 plume number. The ratios of NO_2^+/NO^+ (black data in the lower panel) from the corrected peaks
561 at *m/z* 46 and 30, respectively, are compared to the ratios expected for ammonium nitrate (AN
562 Calibration Ratio, blue horizontal line at 0.49) or organic nitrate (pRONO$_2$ Ratio, green
563 horizontal line at 0.175 which is estimated from the AN calibration ratio using multiple data sets
564 by Day *et al*. (Day et al., 2017)). The measured ratio for most of the flight is more characteristic
565 of organic nitrate than ammonium nitrate.
566
567 We can also employ the comparison of other AMS-measured aerosol components during the
568 individual plumes to assess the possibility of an inorganic nitrate contribution to total measured
569 nitrate. Fig. S5 shows that the in-plume increases in sulfate are correlated with increases in
570 ammonium with an R^2 of 0.4. The observed slope of 5.4 is characteristic of primarily $(NH_4)HSO_4$,
571 which indicates that the sulfate mass is not fully neutralized by ammonium. We note, however,
572 that if the largest observed aerosol nitrate increase is due solely to ammonium nitrate, the
573 ammonium increase would be only 0.11 µg m^{-3}, which would be difficult to discern from the NH$_4$
574 variability of order 0.11 µg m^{-3}. However, the slope is consistent with incomplete neutralization
575 of the sulfate by ammonium, which would make $HNO_{3(g)}$ the more thermodynamically favorable
576 form of inorganic nitrate. Thus, NH_4NO_3 is unlikely to be stable in the aerosol phase under the
577 conditions of these plumes, consistent with the AMS observations.
578

579 A plot of the calculated plume enhancements from the derived apportionment into organic
580 (pRONO$_2$) and inorganic (ammonium) nitrate is shown in Fig. 4. The increases in aerosol nitrate
581 for nearly all of the plumes appear to be mostly due to enhancements in pRONO2. Based on
582 these considerations, we conclude that in-plume pRONO$_2$ mass increases are a consequence
583 (and thus a robust measure) of organic nitrate aerosol produced from NO$_3$ + isoprene. Since
584 each isoprene molecule condensing will have one nitrate group, the ratio of these increases to
585 isoprene loss is a direct measure of the molar organic aerosol yield from NO$_3$-isoprene
586 oxidation.
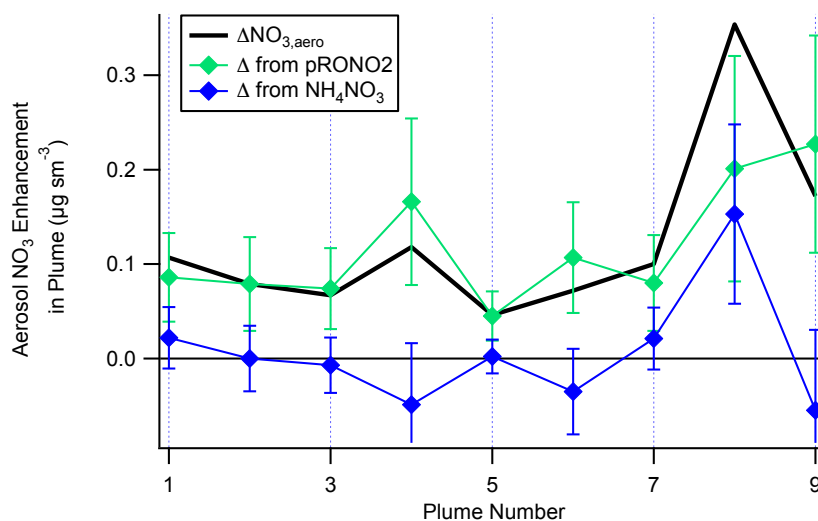
587

588
589 **Figure 4** The contribution of each species to the nitrate enhancements in each of the plumes,
590 showing that the enhancements in most of the plumes are mainly due to enhancements in
591 organic nitrate, with the exception of Plume 8 which had enhancements in both organic and
592 ammonium nitrate. Error bars are estimated from the measurement variability, the UMR
593 corrections to the nitrate signals, apportionment between organic and inorganic nitrate, and the
594 total nitrate uncertainty (see Supplemental Information)

595

596 Table 1 shows the selected plumes to be used for yield analysis. Wherever possible, multiple
597 points have been averaged for in-plume and background isoprene and nitrate aerosol
598 concentrations; in each case the number of points used is indicated and the corresponding
599 standard deviations are reported. In two cases (2:20 and 3:03 plumes), the plumes were so
600 narrow that only a single point was measured in-plume at the 10 s time resolution of the PTR-
601 MS and AMS; for these "single-point" plumes it is not possible to calculate error bars. Error bars
602 were determined using the standard deviations calculated for in-plume and background
603 isoprene and nitrate aerosol concentrations, and propagated through the yield formula detailed
604 in the following section.
605

Table 1. List of plumes used in this NO$_3$ + isoprene SOA yield analysis. For each plume, the delta-values listed indicate the difference between in-plume and outside-plume background in average observed concentration, and the standard deviations (SD) are the propagated error from this subtraction. After each plume number, the numbers of points averaged for isoprene (10 s resolution) and AMS (10 s resolution), respectively, are listed. Because the isoprene data were reported at a lower frequency, these numbers are typically lower to cover the same period of time. Plume numbers annotated with * indicate brief plumes for which only single-point measurements of in-plume aerosol composition were possible. Additional AMS and auxiliary data from each plume is included in the Supplemental Information, Table S3.

plume number [#isop/#AMS]	7/2/13 plume time (UTC)	ΔISOP (ppt) [± SD]	ΔNO$_{3,aero}$ (µg m^{-3}) [± SD]	ΔNO$_3$ from pRONO$_2$ (µg m^{-3}) [± SD]	ΔNO$_3$ from NH$_4$NO$_3$ (µg m^{-3}) [± SD]
	Typical variability (µg m^{-3}):		0.05	0.05	0.05
1 [2/3]	2:18	-335 [128]	0.107 [0.039]	0.086 [0.033]	0.022 [0.012]
2 [*]	2:20	-404	0.079	0.079	0
3 [4/5]	2:21	-228 [121]	0.067 [0.039]	0.074 [0.048]	-0.007 [0.027]
4 [*]	3:03	-453	0.118	0.166	-0.049
5** [3/4]	3:55	-255 [251]	0.046 [0.019]	0.045 [0.026]	0.002 [0.015]
6 [2/2]	4:34	-713 [219]	0.072 [0.031]	0.107 [0.034]	-0.035 [0.029]
7 [5/6]	4:37	-298 [197]	0.100 [0.082]	0.080 [0.077]	0.021 [0.034]
8*** [2/3]	4:39	-443 [75]	0.354 [0.058]	0.201 [0.112]	0.153 [0.057]
9 [7/8]	5:04	-293 [131]	0.172 [0.048]	0.227 [0.056]	-0.055 [0.042]

**Plume 5 has the smallest ΔNO$_{3,aero}$ and may be affected by background pRONO$_2$ variability.

***Plume 8 has a measurable increase in inorganic nitrate as well as organic.

4.2 SOA yield analysis

A **molar** SOA yield refers to the number of molecules of aerosol organic nitrate produced per molecule of isoprene consumed. In order to determine molar SOA yields from the data presented in Table 1, we convert the aerosol organic nitrate mass loading differences to mixing ratio differences (ppt) using the NO$_3$ molecular weight of 62 g mol^{-1}. At standard conditions of 273 K and 1 atm (all aerosol data are reported with this STP definition), 1000 ppt NO$_3$ = 2.77 µg m^{-3}, so each ΔM_{pRONO2} is multiplied by 361 ppt (µg m^{-3})$^{-1}$ to determine this molar yield:

624

$$Y_{SOA,molar} = \frac{(pRONO2_{plume} \pm SD_{pRONO2plume}) - (pRONO2_{bkg} \pm SD_{pRONO2bkg})}{-[(isop_{plume} \pm SD_{isopplume}) - (isop_{bkg} \pm SD_{isopbkg})]} \times \frac{361\ ppt\ NO_3}{\mu g\ m^{-3}}$$ (3)

626
627 The SOA molar yields resulting from this calculation are shown in Table 2, spanning a range of
628 5-28%, with uncertainties indicated based on the SDs in measured AMS and isoprene
629 concentrations. In addition to this uncertainty based on measurement precision and ambient
630 variability, there is an uncertainty of 50% in the AMS derived-organic nitrate mass loadings (see
631 SI) and 25% in the PTR-MS isoprene concentrations (Warneke et al., 2016). The average molar
632 $pRONO_2$ yield across all plumes, with each point weighed by the inverse of its standard
633 deviation and assuming SD = 0.1 for single point plumes, is 9%. (As noted below, the yield
634 appears to increase with plume age, so this average obscures that trend.) An alternate
635 graphical analysis of molar SOA yield from all nine plumes plus one 'null' plume (03:14, in which
636 no isoprene had yet reacted and thus not included in Tables 1 and 2) obtains the same average
637 molar yield of 9% (Fig. 5). Here, the molar yield is the slope of a plot of plume change in
638 $pRONO_2$ vs plume change in isoprene. The slope is determined by a linear fit with points
639 weighted by the square root of the number of AMS data points used to determine in-plume
640 $pRONO_2$ in each case.
641
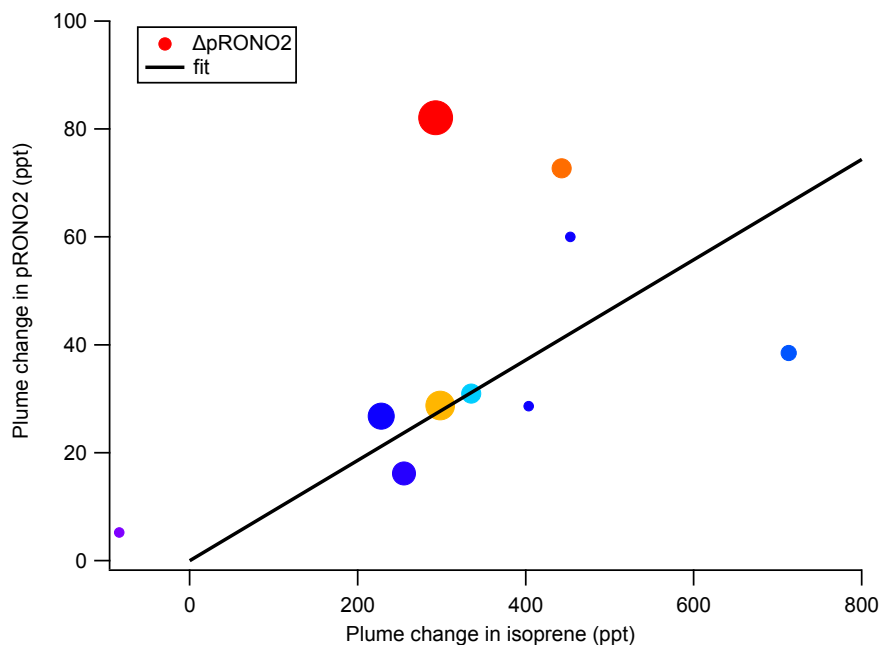
642
Figure 5. SOA molar yield can be determined as the slope of $\Delta pRONO_2$ vs. Δisoprene, both in
644 mixing ratio units. The linear fit is weighted by square root of number of points to determine
645 each in-plume $pRONO_2$, with intercept held at zero. The slope coefficient ± one standard
646 deviation is 0.09298 ± 0.00113. Points are colored by plume age (red = longest), and size
647 scaled by square root of number of points (the point weight used in linear fit). This plot and fit

648   includes the nine plumes listed in Tables 1 and 2, as well as the 03:14 "unreacted" plume (at
649   Δisoprene = -84 ppt.

651   To estimate SOA **mass** yields, we need to make some assumption about the mass of the
652   organic molecules containing the nitrate groups that lead to the observed nitrate aerosol mass
653   increase. The observed changes in organic aerosol are too variable to be simply interpreted as
654   the organic portion of the aerosol organic nitrate molecules. We conservatively assume the
655   organic mass to be approximately double the nitrate mass (62 g mol^{-1}), based on an "average"
656   molecular structure of an isoprene nitrate with 3 additional oxygens: e.g. a tri-hydroxynitrate
657   ($C_5H_{11}O_3$, 119 g mol^{-1}), consistent with 2nd-generation oxidation product structures suggested in
658   Schwantes, et al. (Schwantes et al., 2015). Based on this assumed organic to nitrate ratio, all
659   plumes' expected organic mass increases would be less than the typical variability in organic of
660   0.75 µg m^{-3}. This assumed structure is consistent with oxidation of both double bonds, which
661   appears to be necessary for substantial condensation of isoprene products, and which
662   structures would have calculated vapor pressures sufficiently low to partition to the aerosol
663   phase (Rollins et al., 2009). However, it is difficult to understand how the second double bond
664   would be oxidized unless by another nitrate radical, which would halve these organic to nitrate
665   ratios (assuming the nitrate is retained in the molecules). On the other hand, any organic nitrate
666   aerosol may lose the NO_3 moiety, increasing the organic to nitrate ratio. Given these
667   uncertainties, we use the assumed "average" structure above to guess an associated organic
668   mass of double the nitrate mass. Thus, to estimate SOA mass yield, we multiply the increase in
669   organic nitrate aerosol mass concentration by three (i.e., 2 × ΔM_{pRONO2} + ΔM_{pRONO2}), and divide
670   by the observed decrease in isoprene, converted to µg m^{-3} by multiplying by 329 ppt (µg m^{-3})$^{-1}$,
671   the conversion factor based on isoprene's molecular weight of 68.12 g mol^{-1}.

673   $$Y_{SOA,mass} = \frac{(pRONO2_{plume} \pm SD_{pRONO2plume}) - (pRONO2_{bkg} \pm SD_{pRONO2bkg})}{-[(isop_{plume} \pm SD_{isopplume}) - (isop_{bkg} \pm SD_{isopbkg})]} \times 3 \times \frac{329ppt}{\mu g\ m^{-3}} \qquad (4)$$

675   Note that the SOA mass yield reported here is based on the (assumed) mass of organic aerosol
676   plus the (organo)nitrate aerosol formed in each plume. If instead the yield were calculated using
677   only the assumed increase in **organic** mass (i.e., 2x ΔM_{pRONO2} instead of 3x ΔM_{pRONO2}), which
678   would be consistent with the method used in Rollins, et al. (Rollins et al., 2009) and Brown et al.
679   (Brown et al., 2009), the mass yields would be 2/3 the values reported here. However, since
680   SOA mass yield is typically defined based on the total increase in aerosol mass, we use the
681   definition with the sum of the organic and nitrate mass here.

683   We note also that correlation of in-plume increases in OA with $pRONO_2$ (Fig. 6) point to a
684   substantially larger 5:1 organic-to-nitrate ratio; if this were interpreted as indicating that the
685   average molecular formula of the condensing organic nitrate has 5 times the organic mass as
686   nitrate, this would increase the SOA mass yields reported here. However, due to the
687   aforementioned possibility of additional sources of co-condensing organic aerosol, which led us
688   to avoid using ΔOA in determining SOA yields, we do not consider this to be a direct indication
689   of the molecular formula of the condensing organic nitrate. Including OA in the SOA yield

690   determination, based on this 5:1 slope rather than the assumed 2:1 OA:pRONO$_2$, would give
691   2.5 times larger SOA mass yiels than reported here.
692
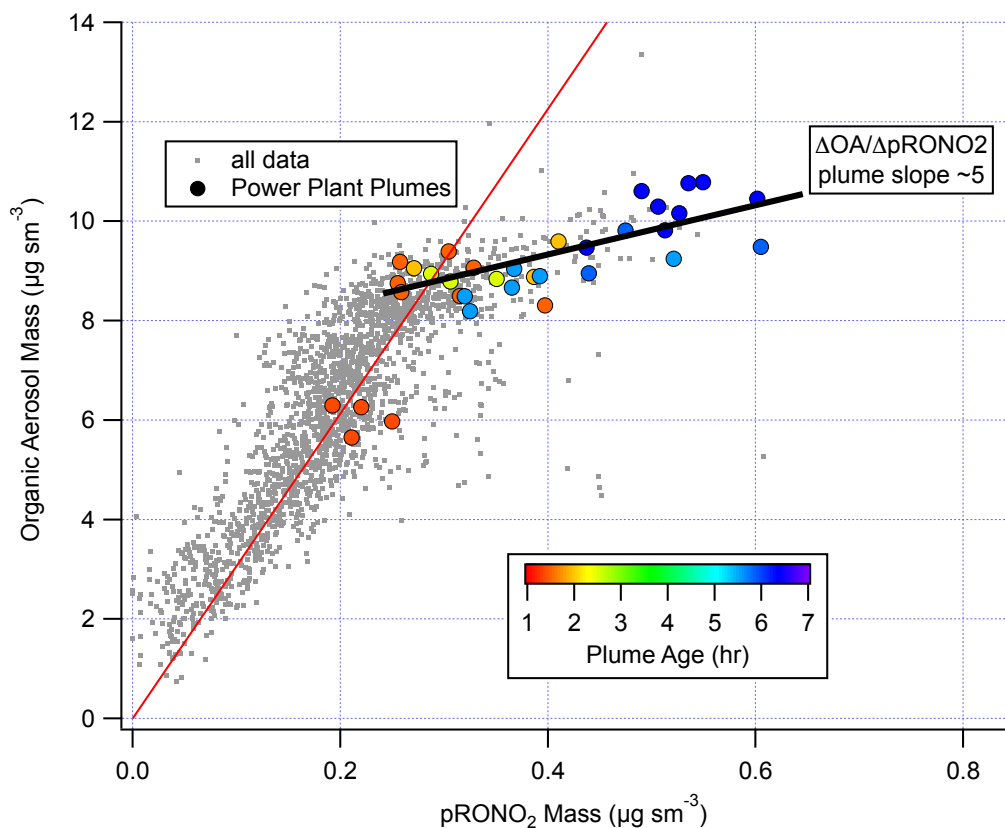
693
694   **Figure 6**. Correlation of organic aerosol mass concentration with pRONO$_2$ mass concentration
695   for the full 2 July flight (grey points and red fit line, fitted slope and thus average OA/pRONO$_2$
696   mass ratio of ~30) and for the points during the selected plumes (colored points, colored by
697   plume age, average OA/pRONO$_2$ mass ratio of ~ 5).

698
699

700 **Table 2.** SOA Yields for each plume observation, estimated plume age, and likely origin. See
701 text for description of uncertainty estimates. For the mass yields, the calculated SOA mass
702 increase includes both the organic and (organo)nitrate aerosol mass; the measurements for OA
703 increases shown in Figure 6 do not include the nitrate mass.

plume number	plume time (UTC)	SOA molar yield (fraction) [± SD]	SOA mass yield (fraction) [± SD]	plume age from O_3/ NO_2 clock assuming S=1 (hours)	Likely NOx origin & altitude (m)
1	7/2/13 2:18	0.09 [0.05]	0.25 [0.14]	2.5	Greene County @ 540 m
2	7/2/13 2:20	0.07	0.21	1.5	*ibid*
3	7/2/13 2:21	0.12 [0.10]	0.32 [0.27]	1.5	*ibid*
4	7/2/13 3:03	0.13	0.36	1.5	Gaston @ 720 m
5	7/2/13 3:55	0.06 [0.07]	0.17 [0.20]	1.4	Miller / Gorgas @ 690 m
6	7/2/13 4:34	0.05 [0.02]	0.15 [0.07]	2	*ibid*
7	7/2/13 4:37	0.10 [0.11]	0.26 [0.31]	5.5	*ibid*
8	7/2/13 4:39	0.16 [0.10]	0.45 [0.26]	5.8	Miller / Gorgas @ 1120 m
9	7/2/13 5:04	0.28 [0.14]	0.77 [0.39]	6.3	Gaston @ 1280 m

704
705

706 **Table 3.** Several caveats to the present SOA yields analysis are listed below, alongside the
707 expected direction each would adjust the estimated yields. Because we do not know whether or
708 how much each process may have occurred in the studied plumes, we cannot quantitatively
709 assess the resulting uncertainties, so we simply list them here. See text above for more detailed
710 discussion.

Process	Effect on determined SOA yield
Organic nitrate aerosol loses NO_3 functional group	Larger, because the non-nitrate OA would not be counted in this analysis
Both double bonds in isoprene are oxidized by NO_3: two nitrates per condensing molecule	Smaller, because the assumed organic to nitrate mass ratio assumes one nitrate per molecule
NO_3 oxidizes daytime isoprene oxidation products (e.g. ISOPOOH) to make new aerosol	Smaller, because this would produce organic nitrate aerosol without corresponding decrease in isoprene, so that some of existing SOA production is mis-attributed to isoprene + NO_3
Assumed organic to nitrate mass ratio is incorrect	Unknown direction of effect, depends on whether assumed ratio is high or low
Daytime-produced IEPOX uptake onto acidic particles	No effect (only changes ΔOA, not nitrate)
Suppression of O_3 + monoterpene or O_3 + isoprene SOA in plumes	No effect (only changes ΔOA, not nitrate)

711
712 Finally, the large range in observed yields can be interpreted by examining the relationship to
713 estimated plume age. Using the slope of O_3 to NO_2 (Eq. 1) to estimate plume age as described
714 above, a weak positive correlation is observed (Table 2, Fig. S4), suggesting that as the plume
715 ages, later-generation chemistry results in greater partitioning to the condensed phase of NO_3 +
716 isoprene organonitrate aerosol products. This is consistent with the observation by Rollins et al.
717 (Rollins et al., 2009) that 2nd-generation oxidation produced substantially higher SOA yields
718 than the oxidation of the first double bond alone, but we note that these mass yields (averaging
719 27%, would be 18% using the organic mass only) are higher than even the largest yield found in
720 that chamber study (14%, used organic mass only).
721
722 We observe increasing SOA yield, from a molar yield of around 10% at 1.5 hours up to 30% at 6
723 hours of aging. The lowest yields observed are found in the most recently emitted plumes,
724 suggesting the interpretation of the higher yields as a consequence of longer aging timescales
725 in the atmosphere.

726 ## 4.3 Mechanistic considerations
727
728 These larger SOA mass yields from field determinations (average 27%) relative to chamber
729 work (12 – 14%, see introduction) may arise for several reasons. We first assess the volatility of
730 assumed first- and second-generation products using group contribution theory in order to
731 predict partitioning. After a single oxidation step, with a representative product assumed to be a

732 C_5 hydroperoxynitrate, the saturation vapor pressure estimated by group contribution theory
733 (Pankow and Asher 2008) at 283 K would be 2.10×10^{-3} Torr ($C^* = 1.7 \times 10^4$ µg m^{-3} for MW =
734 147 g mol^{-1}), while a double-oxidized isoprene molecule (assuming a C_5 dihydroxy dinitrate) has
735 an estimated vapor pressure of 7.95×10^{-8} Torr ($C^* = 1.01$ µg m^{-3} for MW = 226 g mol^{-1}). This
736 supports the conclusion that while the first oxidation step produces compounds too volatile to
737 contribute appreciably to aerosol formation, oxidizing both double bonds of the isoprene
738 molecule is sufficient to produce substantial partitioning, consistent with Rollins et al. (Rollins et
739 al., 2009). This is also true if the second double bond is not oxidized by nitrate (group
740 contribution estimate P_{vap} for a C_5 tri-hydroxy nitrate is 7.7×10^{-8} Torr, $C^* = 0.79$ µg m^{-3} for MW =
741 181 g mol^{-1}). These C^* saturation concentration values suggest that no dimer formation or
742 oligomerization is *required* to produce low-enough volatility products to condense to the aerosol
743 phase; however, such oligomerization would result in more efficient condensation. The fact that
744 Rollins et al. (Rollins et al., 2009) did not observe larger mass yields may indicate that it takes
745 longer than a typical chamber experiment timescale to reach equilibrium, or that this absorptive
746 partitioning model did not accurately capture those experiments, or that substantial loss of
747 semivolatiles to the chamber walls (e.g. (Krechmer et al., 2016)) suppressed apparent yields.
748
749 Determination of yields from ambient atmospheric data differs from chamber determinations in
750 several additional respects. First, ambient measurements do not suffer from wall loss effects,
751 such that no corrections are necessary for loss of aerosol or semi-volatile gases (Matsunaga
752 and Ziemann ‡ 2010, Krechmer et al., 2016). Second, ambient measurements take place on
753 the aging time scale of the atmosphere rather than a time scale imposed by the characteristics
754 of the chamber or the choice of oxidant addition. Third, the typical lifetime of the initially
755 produced nitrooxy-isoprene-RO_2 radical is more representative of the ambient atmosphere
756 rather than a chamber. The unique conditions of a high NO_x power plant plume affect lifetime
757 and fates of peroxy radicals, as described below.
758
759 To help interpret these in-plume peroxy radical lifetimes, a box model calculation using the
760 MCM v3.3.1 chemistry scheme was run (see details in Supplemental Information). This box
761 model shows substantially longer peroxy radical lifetimes during nighttime than daytime,
762 initializing with identical plume-observed conditions. These long peroxy radical lifetimes may
763 have consequences for comparison to chamber experiments: for example, in Schwantes'
764 (Schwantes et al., 2015) chamber experiment on the NO_3 + isoprene reaction mechanism, the
765 HO_2-limited nitrooxy-RO_2 lifetime was at maximum 30 s. In the plumes investigated in this study,
766 peroxy radical lifetimes are predicted to be substantially longer (>200 s early in the night, see
767 Fig. 7), allowing for the possibility of different bimolecular fates, or of unimolecular
768 transformations of the peroxy radicals that may result in lower-volatility products (e.g., auto-
769 oxidation to form highly oxidized molecules (Ehn et al., 2014)).
770
771
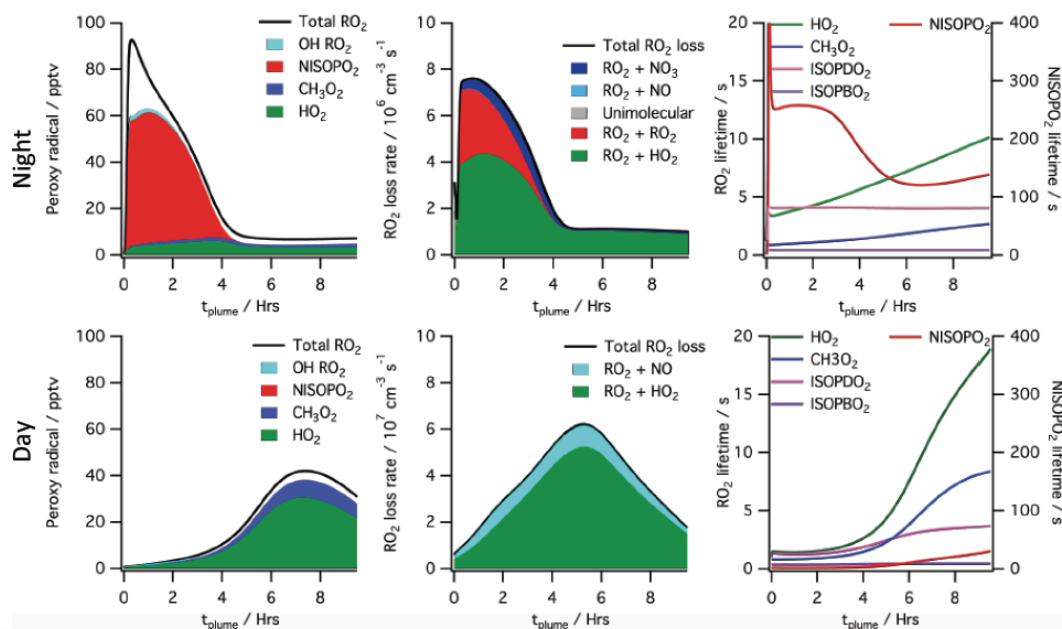
Figure 7. Simulated peroxy radical concentration (left), loss rates (middle), and lifetime (right), using the MCM v3.3.1 chemical mechanism, for conditions typical of a nighttime intercepted power plant plume (top) and the same plume initial conditions run for daytime simulation (bottom, local noon occurs at 5 hrs). Included are total peroxy radical concentration and losses, as well as the highlighted subclasses HO_2, CH_3O_2, total nitrooxy-isoprene-RO_2, and the total hydroxy-isoprene-RO_2 produced from OH oxidation. The righthand panels show HO_2, CH_3O_2 and the dominant hydroxy-isoprene-RO_2 $ISOPBO_2$ and $ISOPDO_2$ (β-hydroxy-peroxy radicals from OH attack at carbons 1 and 4 respectively) lifetime on the left axis and nitrooxy-isoprene-RO_2 on the right axis, showing nighttime lifetimes an order of magnitude longer than daytime for this NO_3 + isoprene derived RO_2 radical ($NISOPO_2$).

The typically assumed major fate of nighttime RO_2 in the atmosphere is reaction with HO_2 to yield a hydroperoxide, NO_3-ROOH. This is shown in the model output above as the green reaction, and is responsible for half of early RO_2 losses in the MCM modeled plume. Schwantes *et al*. (Schwantes et al., 2015) proposed reaction of these nighttime derived hydroperoxides with OH during the following day as a route to epoxides, which in turn can form SOA via reaction with acidic aerosol. Reaction of hydroperoxides with nighttime generated OH may similarly provide a route to SOA through epoxides, albeit more slowly than that due to photochemically generated OH.

The predicted longer nighttime peroxy radical lifetimes may enable unique chemistry. For example, if nitrooxy-isoprene-RO_2 self-reactions are substantially faster than assumed in the MCM, as suggested by Schwantes *et al*. (Schwantes et al., 2015), RO_2+RO_2 reactions may compete with the HO_2 reaction even more than shown in Fig. 7, and dimer formation may be favored at night, yielding lower volatility products. The 5:1 AMS Organic:Nitrate ratio observed in

798   the SOA formed in Rollins et al. (Rollins et al., 2009) , and consistent with aggregated
799   observations reported here, may suggest that in some isoprene units the nitrate is re-released
800   as NO_2 in such oligomerization reactions. We note that this larger organic to nitrate ratio would
801   mean higher SOA mass yields than estimated in Table 2.
802
803   Alternatively, longer nighttime peroxy radical lifetimes may allow sufficient time for
804   intramolecular reactions to produce condensable products. This unimolecular isomerization
805   (auto-oxidation) of initially formed peroxy radicals is a potentially efficient route to low-volatility,
806   highly functionalized products that could result in high aerosol yields. For OH-initiated oxidation
807   of isoprene, laboratory relative rate experiments found the fastest 1,6-H-shift isomerization
808   reaction to occur for the hydroxy-isoprene-RO_2 radical at a rate of 0.002 s^{-1} (Crounse et al.,
809   2011), meaning that peroxy radicals must have an ambient lifetime of >500 s for this process to
810   be dominant. As shown in Fig. 7, the simulated power plant plume peroxy radical lifetimes are
811   long (>200 s), so an isomerization reaction at this rate may play a significant role. However, a
812   recent study has demonstrated that OH-initiated and NO_3-initiated RO_2 radicals from the same
813   precursor VOC can have very different unimolecular reactive fates due to highly structurally
814   sensitive varying rates of reactions of different product channels (Kurtén et al., 2017). A similar
815   theoretical study on the rate of unimolecular autooxidation reactions of nitrooxy-isoprene-RO_2
816   radicals would be valuable to help determine under what conditions such reactions might occur,
817   and this knowledge could be applied to comparing chamber and field SOA yields.

4.4 Two urban plume case studies

819
820   In addition to the nine power plant plumes analyzed above to determine the NO_3 + isoprene
821   SOA molar yield, towards the end of the July 2 flight, the Birmingham urban plume was
822   intercepted twice (around 5:36 am and 6:37 am UTC, Fig. 8). These downwind urban plumes
823   are among the most aged plumes (estimated at 5.2 and 5.8 hours, respectively), but are also
824   substantially more diffuse than the narrow power plant plume intercepts and have lower peak
825    $P(NO_3)$. Nevertheless, we note that these two plumes contain periods of apparent anti-
826   correlation of isoprene and organic nitrate aerosol time series and high apparent SOA molar
827   yields (23%, 19%) and mass yields (62%, 51%), if calculated by the same method as above and
828   omitting the period of vertical profiling in the second plume. Potentially complicating these urban
829   SOA yield determinations is the fact that the inorganic fraction of nitrate was much larger than in
830   the power plant plumes (see Fig. 8). The background isoprene is also somewhat lower in these
831   urban plumes, potentially shifting the NO_3/N_2O_5 fate to reactions other than NO_3 + isoprene (see
832   Fig. S4 in Edwards et al. (Edwards et al., 2017)). The aerosol surface area is not noticeably
833   higher in these urban plumes, which one might expect to lead to a larger contribution of N_2O_5
834   uptake and hydrolysis. In the more complex mix of gases characteristic of an urban plume, we
835   hesitate to attribute these apparent yields exclusively to the NO_3 + isoprene reaction.
836
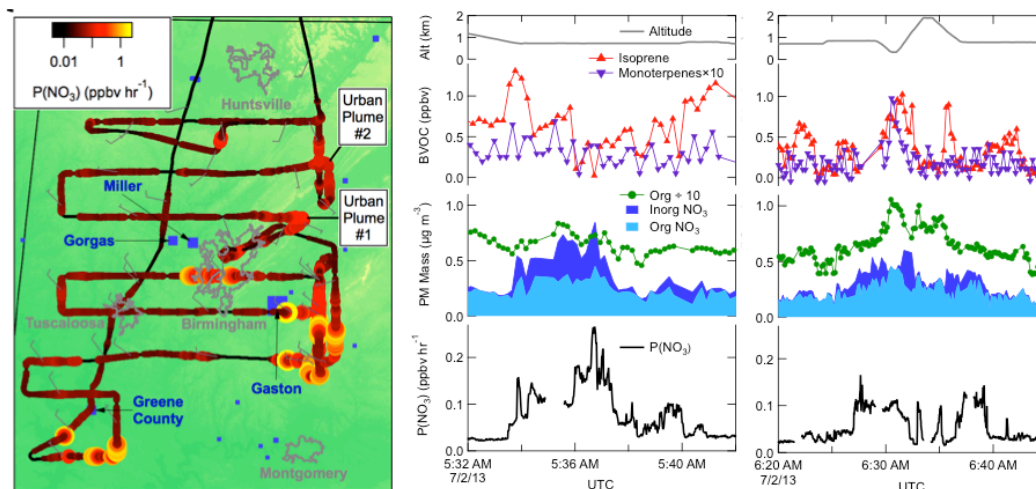
837

838 **Figure 8.** Flight map and time series of two urban plume intercepts, showing anticorrelation of
839 organic nitrate and isoprene. These more diffuse plumes, with lower $P(NO_3)$ and larger
840 inorganic nitrate contribution, make yield determination more uncertain, so we do not include
841 them in the overall yield determination. However, using the same methodology as for the power
842 plant plumes would give similarly high yields for these very aged plumes.

843

844 ## 4.5 Atmospheric implications and needs for future work

845 Because this paper proposes higher SOA yield for the NO_3 + isoprene reaction than measured
846 in chamber studies, we conclude with some discussion of the implications for regional aerosol
847 burdens, and further needs for investigation in the NO_3 + isoprene system.

848

849 Using an isoprene + NO_3 yield parameterization that gave a 12% SOA mass yield at 10 µg m^{-3},
850 Pye et al. (2010) found that adding the NO_3 + isoprene oxidation pathway increased isoprene
851 SOA mass concentrations in the southeastern United States by about 30%, increases of 0.4 to
852 0.6 µg m^{-3}. The larger NO_3 + isoprene SOA mass yields suggested in this paper, with average
853 value of 30%, could double this expected NO_3 radical enhancement of SOA production.
854 Edwards et al. (2017) concluded that the southeast U.S. is currently in transition between NO_x-
855 independent and NO_x-controlled nighttime BVOC oxidation regime. If NO_3-isoprene oxidation is
856 a larger aerosol source than currently understood, and if future NO_x reductions lead to a
857 stronger sensitivity in nighttime BVOC oxidation rates, regional SOA loadings could decrease by
858 a substantial fraction from the typical regional summertime OA loadings of 5 +/- 3 µg m^{-3} (Saha
859 et al., 2017).

860

861 Analysis of the degree of oxidation and chemical composition of NO_3 + isoprene SOA would
862 help to elucidate mechanistic reasons for the different field and lab SOA yields. For example,
863 the potential contribution of the uptake of morning-after OH + NISOPOOH produced epoxides,
864 discussed above in section 4.3, onto existing (acidic) aerosol could be quantified by
865 measurement of these intermediates or their products in the aerosol phase. Assessment of

866 degree of oxidation could help determine whether auto-oxidation mechanisms are active.
867 Because of the potentially large effect on predicted SOA loading in regions of high isoprene
868 emissions, a better mechanistic understanding of these observed yields is crucial.
869

870 **Acknowledgements**
871 JLF gratefully acknowledges funding from the EPA STAR Program (no. RD-83539901) and from
872 the Fulbright U.S. Scholars Program in the Netherlands. PCJ, DAD, and JLJ were partially
873 supported by EPA STAR 83587701-0 and DOE (BER/ASR) DE-SC0016559. This paper has not
874 been formally reviewed by EPA. The views expressed in this document are solely those of the
875 authors, and do not necessarily reflect those of EPA. EPA does not endorse any products or
876 commercial services mentioned in this publication.

877 ## 5 References

878 . "SEAC4RS data." from DOI: 10.5067/Aircraft/SEAC4RS/Aerosol-TraceGas-Cloud.
879 Allan, J. D., K. N. Bower, H. Coe, H. Boudries, J. T. Jayne, M. R. Canagaratna, D. B. Millet, A.
880 H. Goldstein, P. K. Quinn, R. J. Weber and D. R. Worsnop (2004). "Submicron aerosol
881 composition at Trinidad Head, California, during ITCT 2K2: Its relationship with gas phase
882 volatile organic carbon and assessment of instrument performance." Journal of Geophysical
883 Research: Atmospheres **109**(D23): n/a-n/a.
884 Allan, J. D., A. E. Delia, H. Coe, K. N. Bower, M. R. Alfarra, J. L. Jimenez, A. M. Middlebrook, F.
885 Drewnick, T. B. Onasch, M. R. Canagaratna, J. T. Jayne and D. R. Worsnop (2004). "A
886 generalised method for the extraction of chemically resolved mass spectra from Aerodyne
887 aerosol mass spectrometer data." Journal of Aerosol Science **35**(7): 909-922.
888 Atkinson, R., D. L. Baulch, R. A. Cox, J. N. Crowley, R. F. Hampson, R. G. Hynes, M. E. Jenkin,
889 M. J. Rossi and J. Troe (2004). "Evaluated kinetic and photochemical data for atmospheric
890 chemistry: Volume I - gas phase reactions of Ox, HOx, NOx and SOx species." Atmos. Chem.
891 Phys. **4**(6): 1461-1738.
892 Ayres, B. R., H. M. Allen, D. C. Draper, S. S. Brown, R. J. Wild, J. L. Jimenez, D. A. Day, P.
893 Campuzano-Jost, W. Hu, J. de Gouw, A. Koss, R. C. Cohen, K. C. Duffey, P. Romer, K.
894 Baumann, E. Edgerton, S. Takahama, J. A. Thornton, B. H. Lee, F. D. Lopez-Hilfiker, C. Mohr,
895 P. O. Wennberg, T. B. Nguyen, A. Teng, A. H. Goldstein, K. Olson and J. L. Fry (2015).
896 "Organic nitrate aerosol formation via NO_3 + biogenic volatile organic compounds
897 in the southeastern United States." Atmos. Chem. Phys. **15**(23): 13377-13392.
898 Bahreini, R., E. J. Dunlea, B. M. Matthew, C. Simons, K. S. Docherty, P. F. DeCarlo, J. L.
899 Jimenez, C. A. Brock and A. M. Middlebrook (2008). "Design and Operation of a Pressure-
900 Controlled Inlet for Airborne Sampling with an Aerodynamic Aerosol Lens." Aerosol Science and
901 Technology **42**(6): 465-471.
902 Bahreini, R., B. Ervens, A. M. Middlebrook, C. Warneke, J. A. de Gouw, P. F. DeCarlo, J. L.
903 Jimenez, C. A. Brock, J. A. Neuman, T. B. Ryerson, H. Stark, E. Atlas, J. Brioude, A. Fried, J. S.
904 Holloway, J. Peischl, D. Richter, J. Walega, P. Weibring, A. G. Wollny and F. C. Fehsenfeld
905 (2009). "Organic aerosol formation in urban and industrial plumes near Houston and Dallas,
906 Texas." Journal of Geophysical Research: Atmospheres **114**(D7): n/a-n/a.
907 Boyd, C. M., J. Sanchez, L. Xu, A. J. Eugene, T. Nah, W. Y. Tuet, M. I. Guzman and N. L. Ng
908 (2015). "Secondary organic aerosol formation from the β-pinene+NO3 system: effect of humidity
909 and peroxy radical fate." Atmos. Chem. Phys. **15**(13): 7497-7522.
910 Brock, C. A., J. Cozic, R. Bahreini, K. D. Froyd, A. M. Middlebrook, A. McComiskey, J. Brioude,
911 O. R. Cooper, A. Stohl, K. C. Aikin, J. A. de Gouw, D. W. Fahey, R. A. Ferrare, R. S. Gao, W.
912 Gore, J. S. Holloway, G. Hübler, A. Jefferson, D. A. Lack, S. Lance, R. H. Moore, D. M. Murphy,

A. Nenes, P. C. Novelli, J. B. Nowak, J. A. Ogren, J. Peischl, R. B. Pierce, P. Pilewskie, P. K. Quinn, T. B. Ryerson, K. S. Schmidt, J. P. Schwarz, H. Sodemann, J. R. Spackman, H. Stark, D. S. Thomson, T. Thornberry, P. Veres, L. A. Watts, C. Warneke and A. G. Wollny (2011). "Characteristics, sources, and transport of aerosols measured in spring 2008 during the aerosol, radiation, and cloud processes affecting Arctic Climate (ARCPAC) Project." Atmos. Chem. Phys. **11**(6): 2423-2453.

Brock, C. A., N. L. Wagner, B. E. Anderson, A. R. Attwood, A. Beyersdorf, P. Campuzano-Jost, A. G. Carlton, D. A. Day, G. S. Diskin, T. D. Gordon, J. L. Jimenez, D. A. Lack, J. Liao, M. Z. Markovic, A. M. Middlebrook, N. L. Ng, A. E. Perring, M. S. Richardson, J. P. Schwarz, R. A. Washenfelder, A. Welti, L. Xu, L. D. Ziemba and D. M. Murphy (2016). "Aerosol optical properties in the southeastern United States in summer – Part 1: Hygroscopic growth." Atmos. Chem. Phys. **16**(8): 4987-5007.

Brown, S. S., J. A. deGouw, C. Warneke, T. B. Ryerson, W. P. Dubé, E. Atlas, R. J. Weber, R. E. Peltier, J. A. Neuman, J. M. Roberts, A. Swanson, F. Flocke, S. A. McKeen, J. Brioude, R. Sommariva, M. Trainer, F. C. Fehsenfeld and A. R. Ravishankara (2009). "Nocturnal isoprene oxidation over the Northeast United States in summer and its impact on reactive nitrogen partitioning and secondary organic aerosol." Atmos. Chem. Phys. **9**(9): 3027-3042.

Brown, S. S., W. P. Dubé, R. Bahreini, A. M. Middlebrook, C. A. Brock, C. Warneke, J. A. de Gouw, R. A. Washenfelder, E. Atlas, J. Peischl, T. B. Ryerson, J. S. Holloway, J. P. Schwarz, R. Spackman, M. Trainer, D. D. Parrish, F. C. Fehshenfeld and A. R. Ravishankara (2013). "Biogenic VOC oxidation and organic aerosol formation in an urban nocturnal boundary layer: aircraft vertical profiles in Houston, TX." Atmos. Chem. Phys. **13**(22): 11317-11337.

Brown, S. S., W. P. Dubé, P. Karamchandani, G. Yarwood, J. Peischl, T. B. Ryerson, J. A. Neuman, J. B. Nowak, J. S. Holloway, R. A. Washenfelder, C. A. Brock, G. J. Frost, M. Trainer, D. D. Parrish, F. C. Fehsenfeld and A. R. Ravishankara (2012). "Effects of NOxcontrol and plume mixing on nighttime chemical processing of plumes from coal-fired power plants." Journal of Geophysical Research: Atmospheres **117**(D7): n/a-n/a.

Brown, S. S., J. A. Neuman, T. B. Ryerson, M. Trainer, W. P. Dubé, J. S. Holloway, C. Warneke, J. A. de Gouw, S. G. Donnelly, E. Atlas, B. Matthew, A. M. Middlebrook, R. Peltier, R. J. Weber, A. Stohl, J. F. Meagher, F. C. Fehsenfeld and A. R. Ravishankara (2006). "Nocturnal odd-oxygen budget and its implications for ozone loss in the lower troposphere." Geophysical Research Letters **33**(8): n/a-n/a.

Bruns, E. A., V. Perraud, A. Zelenyuk, M. J. Ezell, S. N. Johnson, Y. Yu, D. Imre, B. J. Finlayson-Pitts and M. L. Alexander (2010). "Comparison of FTIR and Particle Mass Spectrometry for the Measurement of Particulate Organic Nitrates." Environmental Science & Technology **44**(3): 1056-1061.

Cai, Y., D. C. Montague, W. Mooiweer-Bryan and T. Deshler (2008). Performance characteristics of the ultra high sensitivity aerosol spectrometer for particles between 55 and 800 nm: Laboratory and field studies.

Calvert, J. G., J. A. Atkinson, J. A. Kerr, S. Madronich, G. K. Moortgat, T. J. Wallington and G. Yarwood (2000). Mechanisms of the atmospheric oxidation of the alkenes. New York, NY, Oxford University Press.

Carlton, A. G., R. W. Pinder, P. V. Bhave and G. A. Pouliot (2010). "To What Extent Can Biogenic SOA be Controlled?" Environmental Science & Technology **44**(9): 3376-3380.

Carlton, A. G., C. Wiedinmyer and J. H. Kroll (2009). "A review of Secondary Organic Aerosol (SOA) formation from isoprene." Atmos. Chem. Phys. **9**(14): 4987-5005.

Crounse, J. D., F. Paulot, H. G. Kjaergaard and P. O. Wennberg (2011). "Peroxy radical isomerization in the oxidation of isoprene." Physical Chemistry Chemical Physics **13**(30): 13607-13613.

962 Darer, A. I., N. C. Cole-Filipiak, A. E. O'Connor and M. J. Elrod (2011). "Formation and Stability
963 of Atmospherically Relevant Isoprene-Derived Organosulfates and Organonitrates."
964 Environmental Science & Technology **45**(5): 1895-1902.
965 Day, D. A., P. Campuzano-Jost, B. B. Palm, W. W. Hu, B. A. Nault, P. J. Wooldridge, R. C.
966 Cohen, K. S. Docherty, J. A. Huffman and J. L. Jimenez (2017). "Evaluation of methods for
967 quantification of bulk particle-phase organic nitrates using real-time aerosol mass spectrometry."
968 in preparation.
969 Dommen, J., H. Hellén, M. Saurer, M. Jaeggi, R. Siegwolf, A. Metzger, J. Duplissy, M. Fierz and
970 U. Baltensperger (2009). "Determination of the Aerosol Yield of Isoprene in the Presence of an
971 Organic Seed with Carbon Isotope Analysis." Environmental Science & Technology **43**(17):
972 6697-6702.
973 Drewnick, F., S. S. Hings, P. DeCarlo, J. T. Jayne, M. Gonin, K. Fuhrer, S. Weimer, J. L.
974 Jimenez, K. L. Demerjian, S. Borrmann and D. R. Worsnop (2005). "A New Time-of-Flight
975 Aerosol Mass Spectrometer (TOF-AMS)—Instrument Description and First Field Deployment."
976 Aerosol Science and Technology **39**(7): 637-658.
977 Dunlea, E. J., P. F. DeCarlo, A. C. Aiken, J. R. Kimmel, R. E. Peltier, R. J. Weber, J. Tomlinson,
978 D. R. Collins, Y. Shinozuka, C. S. McNaughton, S. G. Howell, A. D. Clarke, L. K. Emmons, E. C.
979 Apel, G. G. Pfister, A. van Donkelaar, R. V. Martin, D. B. Millet, C. L. Heald and J. L. Jimenez
980 (2009). "Evolution of Asian aerosols during transpacific transport in INTEX-B." Atmos. Chem.
981 Phys. **9**(19): 7257-7287.
982 Edwards, P. M., K. C. Aikin, W. P. Dube, J. L. Fry, J. B. Gilman, J. A. de Gouw, M. G. Graus, T.
983 F. Hanisco, J. Holloway, G. Hubler, J. Kaiser, F. N. Keutsch, B. M. Lerner, J. A. Neuman, D. D.
984 Parrish, J. Peischl, I. B. Pollack, A. R. Ravishankara, J. M. Roberts, T. B. Ryerson, M. Trainer,
985 P. R. Veres, G. M. Wolfe, C. Warneke and S. S. Brown (2017). "Transition from high- to low-
986 NOx control of night-time oxidation in the southeastern US." Nature Geosci **10**(7): 490-495.
987 Ehn, M., J. A. Thornton, E. Kleist, M. Sipila, H. Junninen, I. Pullinen, M. Springer, F. Rubach, R.
988 Tillmann, B. Lee, F. Lopez-Hilfiker, S. Andres, I.-H. Acir, M. Rissanen, T. Jokinen, S.
989 Schobesberger, J. Kangasluoma, J. Kontkanen, T. Nieminen, T. Kurten, L. B. Nielsen, S.
990 Jorgensen, H. G. Kjaergaard, M. Canagaratna, M. D. Maso, T. Berndt, T. Petaja, A. Wahner, V.-
991 M. Kerminen, M. Kulmala, D. R. Worsnop, J. Wildt and T. F. Mentel (2014). "A large source of
992 low-volatility secondary organic aerosol." Nature **506**(7489): 476-479.
993 Emmerson, K. M. and M. J. Evans (2009). "Comparison of tropospheric gas-phase chemistry
994 schemes for use within global models." Atmos. Chem. Phys. **9**(5): 1831-1845.
995 Farmer, D. K., A. Matsunaga, K. S. Docherty, J. D. Surratt, J. H. Seinfeld, P. J. Ziemann and J.
996 L. Jimenez (2010). "Response of an aerosol mass spectrometer to organonitrates and
997 organosulfates and implications for atmospheric chemistry." Proceedings of the National
998 Academy of Sciences **107**(15): 6670-6675.
999 Fisher, J. A., D. J. Jacob, K. R. Travis, P. S. Kim, E. A. Marais, C. Chan Miller, K. Yu, L. Zhu, R.
1000 M. Yantosca, M. P. Sulprizio, J. Mao, P. O. Wennberg, J. D. Crounse, A. P. Teng, T. B. Nguyen,
1001 J. M. St. Clair, R. C. Cohen, P. Romer, B. A. Nault, P. J. Wooldridge, J. L. Jimenez, P.
1002 Campuzano-Jost, D. A. Day, W. Hu, P. B. Shepson, F. Xiong, D. R. Blake, A. H. Goldstein, P.
1003 K. Misztal, T. F. Hanisco, G. M. Wolfe, T. B. Ryerson, A. Wisthaler and T. Mikoviny (2016).
1004 "Organic nitrate chemistry and its implications for nitrogen budgets in an isoprene- and
1005 monoterpene-rich atmosphere: constraints from aircraft (SEAC4RS) and ground-based (SOAS)
1006 observations in the Southeast US." Atmos. Chem. Phys. **16**(9): 5969-5991.
1007 Fry, J. L., D. C. Draper, K. J. Zarzana, P. Campuzano-Jost, D. A. Day, J. L. Jimenez, S. S.
1008 Brown, R. C. Cohen, L. Kaser, A. Hansel, L. Cappellin, T. Karl, A. Hodzic Roux, A. Turnipseed,
1009 C. Cantrell, B. L. Lefer and N. Grossberg (2013). "Observations of gas- and aerosol-phase
1010 organic nitrates at BEACHON-RoMBAS 2011." Atmos. Chem. Phys. **13**(1): 8585-8605.
1011 Fry, J. L., A. Kiendler-Scharr, A. W. Rollins, T. Brauers, S. S. Brown, H.-P. Dorn, W. P. Dube, H.
1012 Fuchs, A. Mensah, F. Rohrer, R. Tillmann, A. Wahner, P. J. Wooldridge and R. C. Cohen

1013   (2011). "SOA from limonene: role of NO3 in its generation and degradation." Atmospheric
1014   Chemistry and Physics **11**(8): 3879-3894.
1015   Fry, J. L., A. Kiendler-Scharr, A. W. Rollins, P. J. Wooldridge, S. S. Brown, H. Fuchs, W. Dube,
1016   A. Mensah, M. dal Maso, R. Tillmann, H. P. Dorn, T. Brauers and R. C. Cohen (2009). "Organic
1017   nitrate and secondary organic aerosol yield from NO3 oxidation of beta-pinene evaluated using
1018   a gas-phase kinetics/aerosol partitioning model." Atmospheric Chemistry and Physics **9**(4):
1019   1431-1449.
1020   Fry, J. L., C. Koski, K. Bott, R. Hsu-Flanders and M. Hazell (2015). "Downwind particulate
1021   matters: Regulatory implications of secondary aerosol formation from the interaction of nitrogen
1022   oxides and tree emissions." Environmental Science & Policy **50**: 180-190.
1023   Goldstein, A. H., C. D. Koven, C. L. Heald and I. Y. Fung (2009). "Biogenic carbon and
1024   anthropogenic pollutants combine to form a cooling haze over the southeastern United States."
1025   Proceedings of the National Academy of Sciences **106**(22): 8835-8840.
1026   Guenther, A., T. Karl, P. Harley, C. Wiedinmyer, P. I. Palmer and C. Geron (2006). "Estimates
1027   of global terrestrial isoprene emissions using MEGAN (Model of Emissions of Gases and
1028   Aerosols from Nature)." Atmos. Chem. Phys **6**: 3181-3210.
1029   Guo, H., L. Xu, A. Bougiatioti, K. M. Cerully, S. L. Capps, J. R. Hite Jr, A. G. Carlton, S. H. Lee,
1030   M. H. Bergin, N. L. Ng, A. Nenes and R. J. Weber (2015). "Fine-particle water and pH in the
1031   southeastern United States." Atmos. Chem. Phys. **15**(9): 5211-5228.
1032   Hallquist, M., J. C. Wenger, U. Baltensperger, Y. Rudich, D. Simpson, M. Claeys, J. Dommen,
1033   N. M. Donahue, C. George, A. H. Goldstein, J. F. Hamilton, H. Herrmann, T. Hoffmann, Y.
1034   Iinuma, M. Jang, M. E. Jenkin, J. L. Jimenez, A. Kiendler-Scharr, W. Maenhaut, G. McFiggans,
1035   T. F. Mentel, A. Monod, A. S. H. Prévôt, J. H. Seinfeld, J. D. Surratt, R. Szmigielski and J. Wildt
1036   (2009). "The formation, properties and impact of secondary organic aerosol: current and
1037   emerging issues." Atmospheric Chemistry & Physics **9**: 5155-5235.
1038   Hayes, P. L., A. M. Ortega, M. J. Cubison, K. D. Froyd, Y. Zhao, S. S. Cliff, W. W. Hu, D. W.
1039   Toohey, J. H. Flynn, B. L. Lefer, N. Grossberg, S. Alvarez, B. Rappenglück, J. W. Taylor, J. D.
1040   Allan, J. S. Holloway, J. B. Gilman, W. C. Kuster, J. A. de Gouw, P. Massoli, X. Zhang, J. Liu, R.
1041   J. Weber, A. L. Corrigan, L. M. Russell, G. Isaacman, D. R. Worton, N. M. Kreisberg, A. H.
1042   Goldstein, R. Thalman, E. M. Waxman, R. Volkamer, Y. H. Lin, J. D. Surratt, T. E. Kleindienst,
1043   J. H. Offenberg, S. Dusanter, S. Griffith, P. S. Stevens, J. Brioude, W. M. Angevine and J. L.
1044   Jimenez (2013). "Organic aerosol composition and sources in Pasadena, California, during the
1045   2010 CalNex campaign." Journal of Geophysical Research: Atmospheres **118**(16): 9233-9257.
1046   Heald, C. L., D. K. Henze, L. W. Horowitz, J. Feddema, J. F. Lamarque, A. Guenther, P. G.
1047   Hess, F. Vitt, J. H. Seinfeld, A. H. Goldstein and I. Fung (2008). "Predicted change in global
1048   secondary organic aerosol concentrations in response to future climate, emissions, and land
1049   use change." Journal of Geophysical Research: Atmospheres **113**(D5): n/a-n/a.
1050   Henze, D. K. and J. H. Seinfeld (2006). "Global secondary organic aerosol from isoprene
1051   oxidation." Geophysical Research Letters **33**(9).
1052   Hoyle, C., M. Boy, N. Donahue, J. Fry, M. Glasius, A. Guenther, A. Hallar, K. H. Hartz, M.
1053   Petters and T. Petaja (2011). "A review of the anthropogenic influence on biogenic secondary
1054   organic aerosol." Atmospheric Chemistry and Physics **11**(1): 321-343.
1055   Hoyle, C. R., T. Berntsen, G. Myhre and I. S. A. Isaksen (2007). "Secondary organic aerosol in
1056   the global aerosol - chemical transport model Oslo CTM2." Atmospheric Chemistry and Physics
1057   **7**(21): 5675-5694.
1058   Hu, K. S., A. I. Darer and M. J. Elrod (2011). "Thermodynamics and kinetics of the hydrolysis of
1059   atmospherically relevant organonitrates and organosulfates." Atmos. Chem. Phys. **11**(16):
1060   8307-8320.
1061   Hu, W. W., P. Campuzano-Jost, B. B. Palm, D. A. Day, A. M. Ortega, P. L. Hayes, J. E.
1062   Krechmer, Q. Chen, M. Kuwata, Y. J. Liu, S. S. de Sá, K. McKinney, S. T. Martin, M. Hu, S. H.
1063   Budisulistiorini, M. Riva, J. D. Surratt, J. M. St. Clair, G. Isaacman-Van Wertz, L. D. Yee, A. H.

1064 Goldstein, S. Carbone, J. Brito, P. Artaxo, J. A. de Gouw, A. Koss, A. Wisthaler, T. Mikoviny, T.
1065 Karl, L. Kaser, W. Jud, A. Hansel, K. S. Docherty, M. L. Alexander, N. H. Robinson, H. Coe, J.
1066 D. Allan, M. R. Canagaratna, F. Paulot and J. L. Jimenez (2015). "Characterization of a real-
1067 time tracer for isoprene epoxydiols-derived secondary organic aerosol (IEPOX-SOA) from
1068 aerosol mass spectrometer measurements." Atmos. Chem. Phys. **15**(20): 11807-11833.
1069 Jenkin, M. E., J. C. Young and A. R. Rickard (2015). "The MCM v3.3.1 degradation scheme for
1070 isoprene." Atmos. Chem. Phys. **15**(20): 11433-11459.
1071 Jimenez, J. L., M. R. Canagaratna, N. M. Donahue, A. S. H. Prevot, Q. Zhang, J. H. Kroll, P. F.
1072 DeCarlo, J. D. Allan, H. Coe, N. L. Ng, A. C. Aiken, K. S. Docherty, I. M. Ulbrich, A. P. Grieshop,
1073 A. L. Robinson, J. Duplissy, J. D. Smith, K. R. Wilson, V. A. Lanz, C. Hueglin, Y. L. Sun, J. Tian,
1074 A. Laaksonen, T. Raatikainen, J. Rautiainen, P. Vaattovaara, M. Ehn, M. Kulmala, J. M.
1075 Tomlinson, D. R. Collins, M. J. Cubison, E., J. Dunlea, J. A. Huffman, T. B. Onasch, M. R.
1076 Alfarra, P. I. Williams, K. Bower, Y. Kondo, J. Schneider, F. Drewnick, S. Borrmann, S. Weimer,
1077 K. Demerjian, D. Salcedo, L. Cottrell, R. Griffin, A. Takami, T. Miyoshi, S. Hatakeyama, A.
1078 Shimono, J. Y. Sun, Y. M. Zhang, K. Dzepina, J. R. Kimmel, D. Sueper, J. T. Jayne, S. C.
1079 Herndon, A. M. Trimborn, L. R. Williams, E. C. Wood, A. M. Middlebrook, C. E. Kolb, U.
1080 Baltensperger and D. R. Worsnop (2009). "Evolution of Organic Aerosols in the Atmosphere."
1081 Science(5959): 1525-1529.
1082 Kanakidou, M., J. H. Seinfeld, S. N. Pandis, I. Barnes, F. J. Dentener, M. C. Facchini, R. Van
1083 Dingenen, B. Ervens, A. Nenes, C. J. Nielsen, E. Swietlicki, J. P. Putaud, Y. Balkanski, S. Fuzzi,
1084 J. Horth, G. K. Moortgat, R. Winterhalter, C. E. L. Myhre, K. Tsigaridis, E. Vignati, E. G.
1085 Stephanou and J. Wilson (2005). "Organic aerosol and global climate modelling: a review."
1086 Atmospheric Chemistry and Physics **5**: 1053-1123.
1087 Kiendler-Scharr, A., A. A. Mensah, E. Friese, D. Topping, E. Nemitz, A. S. H. Prevot, M. Äijälä,
1088 J. Allan, F. Canonaco, M. Canagaratna, S. Carbone, M. Crippa, M. Dall Osto, D. A. Day, P. De
1089 Carlo, C. F. Di Marco, H. Elbern, A. Eriksson, E. Freney, L. Hao, H. Herrmann, L. Hildebrandt,
1090 R. Hillamo, J. L. Jimenez, A. Laaksonen, G. McFiggans, C. Mohr, C. O'Dowd, R. Otjes, J.
1091 Ovadnevaite, S. N. Pandis, L. Poulain, P. Schlag, K. Sellegri, E. Swietlicki, P. Tiitta, A.
1092 Vermeulen, A. Wahner, D. Worsnop and H. C. Wu (2016). "Ubiquity of organic nitrates from
1093 nighttime chemistry in the European submicron aerosol." Geophysical Research Letters **43**(14):
1094 7735-7744.
1095 Kim, P. S., D. J. Jacob, J. A. Fisher, K. Travis, K. Yu, L. Zhu, R. M. Yantosca, M. P. Sulprizio, J.
1096 L. Jimenez, P. Campuzano-Jost, K. D. Froyd, J. Liao, J. W. Hair, M. A. Fenn, C. F. Butler, N. L.
1097 Wagner, T. D. Gordon, A. Welti, P. O. Wennberg, J. D. Crounse, J. M. St. Clair, A. P. Teng, D.
1098 B. Millet, J. P. Schwarz, M. Z. Markovic and A. E. Perring (2015). "Sources, seasonality, and
1099 trends of southeast US aerosol: an integrated analysis of surface, aircraft, and satellite
1100 observations with the GEOS-Chem chemical transport model." Atmos. Chem. Phys. **15**(18):
1101 10411-10433.
1102 Kleindienst, T. E., M. Lewandowski, J. H. Offenberg, M. Jaoui and E. O. Edney (2007). "Ozone-
1103 isoprene reaction: Re-examination of the formation of secondary organic aerosol." Geophysical
1104 Research Letters **34**(1): n/a-n/a.
1105 Krechmer, J. E., D. Pagonis, P. J. Ziemann and J. L. Jimenez (2016). "Quantification of Gas-
1106 Wall Partitioning in Teflon Environmental Chambers Using Rapid Bursts of Low-Volatility
1107 Oxidized Species Generated in Situ." Environmental Science & Technology **50**(11): 5757-5765.
1108 Kroll, J. H., N. L. Ng, S. M. Murphy, R. C. Flagan and J. H. Seinfeld (2006). "Secondary Organic
1109 Aerosol Formation from Isoprene Photooxidation." Environmental Science & Technology **40**(6):
1110 1869-1877.
1111 Kurtén, T., K. H. Møller, T. B. Nguyen, R. H. Schwantes, P. K. Misztal, L. Su, P. O. Wennberg,
1112 J. L. Fry and H. G. Kjaergaard (2017). "Alkoxy Radical Bond Scissions Explain the Anomalously
1113 Low Secondary Organic Aerosol and Organonitrate Yields From α-Pinene + NO3." The Journal
1114 of Physical Chemistry Letters: 2826-2834.

Lee, B. H., C. Mohr, F. D. Lopez-Hilfiker, A. Lutz, M. Hallquist, L. Lee, P. Romer, R. C. Cohen, S. Iyer, T. Kurtén, W. Hu, D. A. Day, P. Campuzano-Jost, J. L. Jimenez, L. Xu, N. L. Ng, H. Guo, R. J. Weber, R. J. Wild, S. S. Brown, A. Koss, J. de Gouw, K. Olson, A. H. Goldstein, R. Seco, S. Kim, K. McAvey, P. B. Shepson, T. Starn, K. Baumann, E. S. Edgerton, J. Liu, J. E. Shilling, D. O. Miller, W. Brune, S. Schobesberger, E. L. D'Ambro and J. A. Thornton (2016). "Highly functionalized organic nitrates in the southeast United States: Contribution to secondary organic aerosol and reactive nitrogen budgets." Proceedings of the National Academy of Sciences **113**(6): 1516-1521.

Lelieveld, J., J. S. Evans, M. Fnais, D. Giannadaki and A. Pozzer (2015). "The contribution of outdoor air pollution sources to premature mortality on a global scale." Nature **525**(7569): 367-371.

Lerner, B. M., J. B. Gilman, K. C. Aikin, E. L. Atlas, P. D. Goldan, M. Graus, R. Hendershot, G. A. Isaacman-VanWertz, A. Koss, W. C. Kuster, R. A. Lueb, R. J. McLaughlin, J. Peischl, D. Sueper, T. B. Ryerson, T. W. Tokarek, C. Warneke, B. Yuan and J. A. de Gouw (2017). "An improved, automated whole air sampler and gas chromatography mass spectrometry analysis system for volatile organic compounds in the atmosphere." Atmos. Meas. Tech. **10**(1): 291-313.

Liu, J., E. L. D'Ambro, B. H. Lee, F. D. Lopez-Hilfiker, R. A. Zaveri, J. C. Rivera-Rios, F. N. Keutsch, S. Iyer, T. Kurten, Z. Zhang, A. Gold, J. D. Surratt, J. E. Shilling and J. A. Thornton (2016). "Efficient Isoprene Secondary Organic Aerosol Formation from a Non-IEPOX Pathway." Environmental Science & Technology **50**(18): 9872-9880.

Marais, E. A., D. J. Jacob, J. L. Jimenez, P. Campuzano-Jost, D. A. Day, W. Hu, J. Krechmer, L. Zhu, P. S. Kim, C. C. Miller, J. A. Fisher, K. Travis, K. Yu, T. F. Hanisco, G. M. Wolfe, H. L. Arkinson, H. O. T. Pye, K. D. Froyd, J. Liao and V. F. McNeill (2016). "Aqueous-phase mechanism for secondary organic aerosol formation from isoprene: application to the southeast United States and co-benefit of SO2 emission controls." Atmos. Chem. Phys. **16**(3): 1603-1618.

Marcolli, C., M. R. Canagaratna, D. R. Worsnop, R. Bahreini, J. A. de Gouw, C. Warneke, P. D. Goldan, W. C. Kuster, E. J. Williams, B. M. Lerner, J. M. Roberts, J. F. Meagher, F. C. Fehsenfeld, M. Marchewka, S. B. Bertman and A. M. Middlebrook (2006). "Cluster Analysis of the Organic Peaks in Bulk Mass Spectra Obtained During the 2002 New England Air Quality Study with an Aerodyne Aerosol Mass Spectrometer." Atmos. Chem. Phys. **6**(12): 5649-5666.

Matsunaga, A. and P. J. Ziemann ‡ (2010). "Gas-Wall Partitioning of Organic Compounds in a Teflon Film Chamber and Potential Effects on Reaction Product and Aerosol Yield Measurements." Aerosol Science and Technology **44**(10): 881-892.

Middlebrook, A. M., R. Bahreini, J. L. Jimenez and M. R. Canagaratna (2012). "Evaluation of Composition-Dependent Collection Efficiencies for the Aerodyne Aerosol Mass Spectrometer using Field Data." Aerosol Science and Technology **46**(3): 258-271.

Myhre, G., D. Shindell, F.-M. Bréon, W. Collins, J. Fuglestvedt, J. Huang, D. Koch, J.-F. Lamarque, D. Lee, B. Mendoza, T. Nakajima, A. Robock, G. Stephens, T. Takemura and H. Zhang (2013). Anthropogenic And Natural Radiative Forcing, in Climate Change 2013: The Physical Science Basis. Contribution of Working Group I to the Fifth Assessment Report of the Intergovernmental Panel on Climate Change. T. F. Stocker, D. Qin, G.-K. Plattner et al. New York, NY, USA, Cambridge University Press**:** 659-740.

Ng, N. L., S. S. Brown, A. T. Archibald, E. Atlas, R. C. Cohen, J. N. Crowley, D. A. Day, N. M. Donahue, J. L. Fry, H. Fuchs, R. J. Griffin, M. I. Guzman, H. Herrmann, A. Hodzic, Y. Iinuma, J. L. Jimenez, A. Kiendler-Scharr, B. H. Lee, D. J. Luecken, J. Mao, R. McLaren, A. Mutzel, H. D. Osthoff, B. Ouyang, B. Picquet-Varrault, U. Platt, H. O. T. Pye, Y. Rudich, R. H. Schwantes, M. Shiraiwa, J. Stutz, J. A. Thornton, A. Tilgner, B. J. Williams and R. A. Zaveri (2017). "Nitrate radicals and biogenic volatile organic compounds: oxidation, mechanisms, and organic aerosol." Atmos. Chem. Phys. **17**(3): 2103-2162.

Ng, N. L., A. J. Kwan, J. D. Surratt, A. W. H. Chan, P. S. Chhabra, A. Sorooshian, H. O. T. Pye, J. D. Crounse, P. O. Wennberg, R. C. Flagan and J. H. Seinfeld (2008). "Secondary organic

aerosol (SOA) formation from reaction of isoprene with nitrate radicals (NO3)." Atmos. Chem. Phys. **8**: 4117-4140.

Palm, B. B., P. Campuzano-Jost, D. A. Day, A. M. Ortega, J. L. Fry, S. S. Brown, K. J. Zarzana, W. Dube, N. L. Wagner, D. C. Draper, L. Kaser, W. Jud, T. Karl, A. Hansel, C. Gutiérrez-Montes and J. L. Jimenez (2017). "Secondary organic aerosol formation from in situ OH, O3, and NO3 oxidation of ambient forest air in an oxidation flow reactor." Atmos. Chem. Phys. **17**(8): 5331-5354.

Pankow, J. F. and W. E. Asher (2008). "SIMPOL.1: a simple group contribution method for predicting vapor pressures and enthalpies of vaporization of multifunctional organic compounds." Atmospheric Chemistry and Physics **8**(10): 2773-2796.

Peischl, J., T. B. Ryerson, J. S. Holloway, D. D. Parrish, M. Trainer, G. J. Frost, K. C. Aikin, S. S. Brown, W. P. Dubé, H. Stark and F. C. Fehsenfeld (2010). "A top-down analysis of emissions from selected Texas power plants during TexAQS 2000 and 2006." Journal of Geophysical Research: Atmospheres **115**(D16): n/a-n/a.

Pye, H., A. Chan, M. Barkley and J. Seinfeld (2010). "Global modeling of organic aerosol: the importance of reactive nitrogen (NO_x and NO_3)." Atmospheric Chemistry and Physics **10**(22): 11261-11276.

Pye, H. O. T., D. J. Luecken, L. Xu, C. M. Boyd, N. L. Ng, K. R. Baker, B. R. Ayres, J. O. Bash, K. Baumann, W. P. L. Carter, E. Edgerton, J. L. Fry, W. T. Hutzell, D. B. Schwede and P. B. Shepson (2015). "Modeling the Current and Future Roles of Particulate Organic Nitrates in the Southeastern United States." Environmental Science & Technology **49**(24): 14195-14203.

Rollins, A. W., E. C. Browne, K. E. Min, S. E. Pusede, P. J. Wooldridge, D. R. Gentner, A. H. Goldstein, S. Liu, D. A. Day, L. M. Russell and R. C. Cohen (2012). "Evidence for NOx Control over Nighttime SOA Formation." Science **337**(6099): 1210.

Rollins, A. W., A. Kiendler-Scharr, J. L. Fry, T. Brauers, S. S. Brown, H.-P. Dorn, W. P. Dube, H. Fuchs, A. Mensah, T. F. Mentel, F. Rohrer, R. Tillmann, R. Wegener, P. J. Wooldridge and R. C. Cohen (2009). "Isoprene oxidation by nitrate radical: alkyl nitrate and secondary organic aerosol yields." Atmos. Chem. Phys. **9**: 6685-6703.

Romer, P. S., K. C. Duffey, P. J. Wooldridge, H. M. Allen, B. R. Ayres, S. S. Brown, W. H. Brune, J. D. Crounse, J. de Gouw, D. C. Draper, P. A. Feiner, J. L. Fry, A. H. Goldstein, A. Koss, P. K. Misztal, T. B. Nguyen, K. Olson, A. P. Teng, P. O. Wennberg, R. J. Wild, L. Zhang and R. C. Cohen (2016). "The lifetime of nitrogen oxides in an isoprene-dominated forest." Atmos. Chem. Phys. **16**(12): 7623-7637.

Saha, P. K., A. Khlystov, K. Yahya, Y. Zhang, L. Xu, N. L. Ng and A. P. Grieshop (2017). "Quantifying the volatility of organic aerosol in the southeastern US." Atmos. Chem. Phys. **17**(1): 501-520.

Schwantes, R. H., A. P. Teng, T. B. Nguyen, M. M. Coggon, J. D. Crounse, J. M. St. Clair, X. Zhang, K. A. Schilling, J. H. Seinfeld and P. O. Wennberg (2015). "Isoprene NO3 Oxidation Products from the RO2 + HO2 Pathway." The Journal of Physical Chemistry A **119**(40): 10158-10171.

Spracklen, D. V., J. L. Jimenez, K. S. Carslaw, D. R. Worsnop, M. J. Evans, G. W. Mann, Q. Zhang, M. R. Canagaratna, J. Allan, H. Coe, G. McFiggans, A. Rap and P. Forster (2011). "Aerosol mass spectrometer constraint on the global secondary organic aerosol budget." Atmos. Chem. Phys. **11**(23): 12109-12136.

Surratt, J. D., A. W. H. Chan, N. C. Eddingsaas, M. N. Chan, C. L. Loza, A. J. Kwan, S. P. Hersey, R. C. Flagan, P. O. Wennberg and J. H. Seinfeld (2010). "Reactive intermediates revealed in secondary organic aerosol formation from isoprene." Proceedings of the National Academy of Sciences **107**(15): 6640-6645.

Takegawa, N., T. Miyakawa, K. Kawamura and Y. Kondo (2007). "Contribution of Selected Dicarboxylic and ω-Oxocarboxylic Acids in Ambient Aerosol to the m/z 44 Signal of an Aerodyne Aerosol Mass Spectrometer." Aerosol Science and Technology **41**(4): 418-437.

Toon, O. B., H. Maring, J. Dibb, R. Ferrare, D. J. Jacob, E. J. Jensen, Z. J. Luo, G. G. Mace, L. L. Pan, L. Pfister, K. H. Rosenlof, J. Redemann, J. S. Reid, H. B. Singh, A. M. Thompson, R. Yokelson, P. Minnis, G. Chen, K. W. Jucks and A. Pszenny (2016). "Planning, implementation, and scientific goals of the Studies of Emissions and Atmospheric Composition, Clouds and Climate Coupling by Regional Surveys (SEAC4RS) field mission." Journal of Geophysical Research: Atmospheres **121**(9): 4967-5009.

Warneke, C., M. Trainer, J. A. de Gouw, D. D. Parrish, D. W. Fahey, A. R. Ravishankara, A. M. Middlebrook, C. A. Brock, J. M. Roberts, S. S. Brown, J. A. Neuman, B. M. Lerner, D. Lack, D. Law, G. Hübler, I. Pollack, S. Sjostedt, T. B. Ryerson, J. B. Gilman, J. Liao, J. Holloway, J. Peischl, J. B. Nowak, K. C. Aikin, K. E. Min, R. A. Washenfelder, M. G. Graus, M. Richardson, M. Z. Markovic, N. L. Wagner, A. Welti, P. R. Veres, P. Edwards, J. P. Schwarz, T. Gordon, W. P. Dube, S. A. McKeen, J. Brioude, R. Ahmadov, A. Bougiatioti, J. J. Lin, A. Nenes, G. M. Wolfe, T. F. Hanisco, B. H. Lee, F. D. Lopez-Hilfiker, J. A. Thornton, F. N. Keutsch, J. Kaiser, J. Mao and C. D. Hatch (2016). "Instrumentation and measurement strategy for the NOAA SENEX aircraft campaign as part of the Southeast Atmosphere Study 2013." Atmos. Meas. Tech. **9**(7): 3063-3093.

Wilson, J. C., B. G. Lafleu, H. Hilbert, W. R. Seebaugh, J. Fox, D. W. Gesler, C. A. Brock, B. J. Huebert and J. Mullen (2004). "Function and Performance of a Low Turbulence Inlet for Sampling Supermicron Particles from Aircraft Platforms." Aerosol Science and Technology **38**(8): 790-802.

Worton, D. R., J. D. Surratt, B. W. LaFranchi, A. W. H. Chan, Y. Zhao, R. J. Weber, J.-H. Park, J. B. Gilman, J. de Gouw, C. Park, G. Schade, M. Beaver, J. M. S. Clair, J. Crounse, P. Wennberg, G. M. Wolfe, S. Harrold, J. A. Thornton, D. K. Farmer, K. S. Docherty, M. J. Cubison, J.-L. Jimenez, A. A. Frossard, L. M. Russell, K. Kristensen, M. Glasius, J. Mao, X. Ren, W. Brune, E. C. Browne, S. E. Pusede, R. C. Cohen, J. H. Seinfeld and A. H. Goldstein (2013). "Observational Insights into Aerosol Formation from Isoprene." Environmental Science & Technology **47**(20): 11403-11413.

Xie, Y., F. Paulot, W. P. L. Carter, C. G. Nolte, D. J. Luecken, W. T. Hutzell, P. O. Wennberg, R. C. Cohen and R. W. Pinder (2013). "Understanding the impact of recent advances in isoprene photooxidation on simulations of regional air quality." Atmos. Chem. Phys. **13**(16): 8439-8455.

Xu, L., H. Guo, C. M. Boyd, M. Klein, A. Bougiatioti, K. M. Cerully, J. R. Hite, G. Isaacman-VanWertz, N. M. Kreisberg, C. Knote, K. Olson, A. Koss, A. H. Goldstein, S. V. Hering, J. de Gouw, K. Baumann, S.-H. Lee, A. Nenes, R. J. Weber and N. L. Ng (2015). "Effects of anthropogenic emissions on aerosol formation from isoprene and monoterpenes in the southeastern United States." Proceedings of the National Academy of Sciences **112**(1): 37-42.

Xu, L., S. Suresh, H. Guo, R. J. Weber and N. L. Ng (2015). "Aerosol characterization over the southeastern United States using high-resolution aerosol mass spectrometry: spatial and seasonal variation of aerosol composition and sources with a focus on organic nitrates." Atmos. Chem. Phys. **15**(13): 7307-7336.

Zhang, H., L. D. Yee, B. H. Lee, M. P. Curtis, D. R. Worton, G. Isaacman-VanWertz, J. H. Offenberg, M. Lewandowski, T. E. Kleindienst, M. R. Beaver, A. L. Holder, W. A. Lonneman, K. S. Docherty, M. Jaoui, H. O. T. Pye, W. Hu, D. A. Day, P. Campuzano-Jost, J. L. Jimenez, H. Guo, R. J. Weber, J. de Gouw, A. R. Koss, E. S. Edgerton, W. Brune, C. Mohr, F. D. Lopez-Hilfiker, A. Lutz, N. M. Kreisberg, S. R. Spielman, S. V. Hering, K. R. Wilson, J. A. Thornton and A. H. Goldstein (2018). "Monoterpenes are the largest source of summertime organic aerosol in the southeastern United States." Proceedings of the National Academy of Sciences **115**(9): 2038.

Zhang, Q., M. R. Alfarra, D. R. Worsnop, J. D. Allan, H. Coe, M. R. Canagaratna and J. L. Jimenez (2005). "Deconvolution and Quantification of Hydrocarbon-like and Oxygenated Organic Aerosols Based on Aerosol Mass Spectrometry." Environmental Science & Technology **39**(13): 4938-4952.

1268 Zhang, Q., J. L. Jimenez, M. R. Canagaratna, J. D. Allan, H. Coe, I. Ulbrich, M. R. Alfarra, A.
1269 Takami, A. M. Middlebrook, Y. L. Sun, K. Dzepina, E. Dunlea, K. Docherty, P. F. DeCarlo, D.
1270 Salcedo, T. Onasch, J. T. Jayne, T. Miyoshi, A. Shimono, S. Hatakeyama, N. Takegawa, Y.
1271 Kondo, J. Schneider, F. Drewnick, S. Borrmann, S. Weimer, K. Demerjian, P. Williams, K.
1272 Bower, R. Bahreini, L. Cottrell, R. J. Griffin, J. Rautiainen, J. Y. Sun, Y. M. Zhang and D. R.
1273 Worsnop (2007). "Ubiquity and dominance of oxygenated species in organic aerosols in
1274 anthropogenically-influenced Northern Hemisphere midlatitudes." Geophysical Research Letters
1275 **34**(13): L13801.
1276 Zhang, Q., C. O. Stanier, M. R. Canagaratna, J. T. Jayne, D. R. Worsnop, S. N. Pandis and J.
1277 L. Jimenez (2004). "Insights into the Chemistry of New Particle Formation and Growth Events in
1278 Pittsburgh Based on Aerosol Mass Spectrometry." Environmental Science & Technology **38**(18):
1279 4797-4809.
1280 Zheng, Y., N. Unger, A. Hodzic, L. Emmons, C. Knote, S. Tilmes, J. F. Lamarque and P. Yu
1281 (2015). "Limited effect of anthropogenic nitrogen oxides on secondary organic aerosol
1282 formation." Atmos. Chem. Phys. **15**(23): 13487-13506.
1283
1284
1285